



**IZMIR DEMOCRACY UNIVERSITY**

# **NATURAL & APPLIED SCIENCES JOURNAL**

**IDUNAS**

**E-ISSN: 2645-9000**

**Year: 2019**

**Volume: 2, Issue: 1**

**Table of Contents**

	Sayfa
1. Review Article	1
a. Plasma Polymerized Films for Mass Sensitive Biosensors	1
b. Altering Surface Topography of Electrospun Fibers	8
c. Biochips for Physical Exercise Studies	15
2. Research Article	27
a. Photochemical Reaction of Metal Carbonyls [M(CO) <sub>6</sub> (M= Cr, Mo, W)] with 2-acetyl-5- chlorothiophenemethanesulfonylhydrazone	27
b. A Bioactive (2R, 3R)-dihydroflavonol-3-O- $\alpha$ -L-rhamnoside from Bracystelma togoense Schltr	32

# Plasma Polymerized Films for Mass Sensitive Biosensors

Gizem Kaleli Can<sup>1</sup>, Selma Mutlu<sup>2</sup> Mehmet Mutlu<sup>3</sup>

## Abstract

Mass sensitive biosensors represent promising tool that used in many areas such as biomedical applications, food, environmental, military and in other fields instead of conventional methods. However, surface modifications are needed to design this rapid and reliable sensors. Plasma polymerization is a commonly used technology which offers easily-controllable, environmentally friendly, and inexpensive processing of various materials when compared to the wet chemical methods. This review includes working principle of mass sensitive biosensors, surface modification of piezoelectric crystals by plasma technology and applications of these crystals as a mass sensitive biosensor in biomedical applications.

## Keywords

Mass sensitive biosensor; quartz crystal microbalance; quartz tuning fork; plasma polymerization; biomedical application.

<sup>1</sup>Plasma Aided Biomedical Research Group (pabmed), Department of Biomedical Engineering, İzmir Democracy University, İzmir 35140, Turkey

<sup>2</sup>Hacettepe University, Engineering Faculty, Department of Chemical Engineering, Beytepe Campus, 06800 Ankara, Turkey

<sup>3</sup>Plasma Aided Biomedical Research Group (pabmed), Department of Biomedical Engineering, TOBB University of Economics and Technology, Ankara 06560, Turkey

\*Corresponding Author: gizem.kalelican@idu.edu.tr

Manuscript received date: June 18, 2019

Accept Date: June 28, 2019

Published Date: June 30, 2019.

## 1. INTRODUCTION

The development of the microprocessor technology and biotechnology have affected the growth rate of biosensor technology [1-2]. Biosensor technology can be used in different areas like biomedical applications, food, environmental, military and etc [2-6]. Considering biomedical applications in particular, target analytes that are indicators of a disease, biological and chemical contaminants or disease-causing micro-organisms should be determined for disease monitoring [7]. Conventional methods used during the detection of these markers have some drawbacks arisen from a series of time-consuming procedure requirement and the usage of complex devices including separative techniques coupled to various detectors such as GC, HPLC, MS, UV and etc. when compared with biosensors [6,8-9]. Additionally, trained personnel are needed to operate time-consuming and complex conventional systems. Due to the demand for rapid, sensitive, selective and accurate methods to detect these target analytes, the development of biosensors became crucial [10].

In biosensors, there are five different transduction system which is known as electrochemical, electrical, piezoelectric (mass-sensitive), thermometric (calorimetric) or optical biosensors [11]. Among these types of biosensors, mass sensitive biosensors are used in many studies due to their high sensitivity, selectivity, label-free operation and low cost [6]. Quartz crystal microbalance (QCM) is the most preferred type of crystal used in mass-sensitive biosensors.

The working principle of QCM can be summarized that the damping in oscillation frequency is proportional with the adsorption of material on the surface of the crystals. It is reported that when an 9 MHz of AT-cut quartz crystal is used as a crystal, the adsorption of mass about 1 ng changes frequency shift of 1 Hz [12-13]. In recent years, the quartz tuning fork (QTF), which has the same working principle as QCM, has shown that it can be an alternative to QCM by drawing attention to its high sensitivity due to its high-quality factor (QF 10000-7000), high frequency stability, sharp frequency response, repeatability in measurements, convenience for mass detection and low cost. These features of QTF, both quartz and fork-like geometry, allow it to pass in front of silicon cantilever and QCM as an inverter. To obtain mass sensitive sensor with good performance for both

crystals, a properly designed biosensor is essential [14].

Surface modification of piezoelectric crystal is crucial step to turn crystals sensing platform to bio-sensing. Many polymeric layers such as cellulose acetate, polyurethane, polystyrene, polyethylene amine, polybutyl methacrylate, polyvinyl formal/ethylal, polyvinylalcohol, and polyethyleneimine have been used for the creation of interface for immobilization of bioreceptor [15-22]. Additionally, many coating methods like silanization, immobilization on the pre-coated crystal, entrapment, or cross-linking methods are used to immobilize bioreceptor such as antibody, aptamer and nucleic acids onto the quartz crystal [6, 16, 18-20, 22-24]. However, at the end of these techniques, thicker films are obtained on the crystals' surfaces which diminishes performance by mass overload, and create a harsh environment, which reduces biological activity.

Nowadays, plasma technologies have been started to be used for the modification of the surface of the quartz crystal [14, 19, 25-32]. This technique give chance to cover the crystal surfaces with control film growth down to the angstrom (Å) scale with uniform coating, while preserving the bulk properties of the substrate material. The obtained layer enhances QCM sensitivity and the immobilization capacity of bioactive agents by obtaining functional groups on recognition layers [22, 28, 33].

In this review, the principle of detection, surface modification of piezoelectric crystals by plasma technology and applications of these crystals as a mass sensitive biosensor in biomedical applications are summarized in concept of the theory and the literature in this field.

## 2. Working Principle of Mass Sensitive Biosensors

In both QCM and QTF biosensors, biological component is quantified by measuring the frequency change, which corresponds to a mass change of the sensor surface. In this sensor type, no potentially hazardous-labeled materials are needed to be used [34].

### 2.1 Detection Scheme of Quartz Crystal Microbalance

Quartz crystal placed in QCM device as a transducer. The preparation of this transducer is achieved by sandwiching of a quartz crystal wafer between two metal electrodes like gold, silver, aluminum, or nickel [35]. Then, an external oscillator circuit are connected to the electrodes and this circuit drives the quartz crystal at its resonant frequency. The resonant frequency of the crystal is directly based on the properties of crystal like the cutting edge, thickness and etc. The quartz plates are used as a biosensor are mostly 5, 9, or 10 MHz AT-cut quartz crystal.

The detection of biological molecule by quartz crystal microbalance (QCM) depends on the measurement of the mass changes and physical properties of thin layers deposited on the crystal surfaces [36-38]. Therefore, these highly precise and stable quartz crystal is a good transducer to be used as a biosensor by monitoring its frequency changes.

Sauerbrey described the working principle of the sensor for the gaseous phase by the relation between the mass loading on quartz crystals and the corresponding change in resonant frequency of the crystal [39]:

$$\Delta f = - 2.f_0^2 \Delta m/A (\rho_q \mu_q)^{1/2}$$

where  $\Delta f$  is the frequency change of the crystal resonance,  $f_0$  is the fundamental frequency of the crystal (in Hz),  $A$  is the surface area (in  $cm^2$ ),  $\Delta m$  is the deposited mass (in g),  $\rho_q$  and  $\mu_q$  is the properties of the density and the shear modulus of crystal, respectively.

By inserting the values of properties (density,  $\rho_q=2.648 \text{ g cm}^{-3}$ ; shear modulus,  $\mu_q=2.987 \times 10^{11} \text{ g cm}^{-1} \text{ s}^{-2}$ ) for an AT cut crystal, the above relationship can be rearranged as:

$$\Delta f = - 2.27 \times 10^{-6} f_0^2 \Delta m/A$$

The Sauerbrey equation gives the frequency shift measured in air corresponding the coated materials. The equation is modified for the frequency measurement in liquid phase due to bulk liquid properties like conductivity, viscosity, density and dielectric constant. In the liquid phase, the frequency shifts are determined by the Bruckenstein-Shay and Kanazawa-Gordon's equation as follows [31-32]:

$$\Delta f = - f_0^{3/2} (\rho_L \eta_L / \pi \rho_q \mu_q)^{1/2}$$

where  $\eta_L$  and  $\rho_L$  are the absolute viscosity and density of the liquid, respectively [6].

### 2.2 Detection Scheme of Quartz Tuning Fork

Quartz tuning fork has become a widely used component in frequency measurement due to their high stability, quality factor, accuracy and low power consumption. These forks have replaced the mechanical pendulum and spring used in watches since the late 1960s, allowing the production of more stable watches. The key component of these high-stability watches, QTF, is manufactured by mass production at low cost, making QTF use even more attractive [42-51].

Nowadays, QTFs have been started to be used as an alternative to microfabricated silicone in atomic force microscopy cantilevers. However, QTF is one step ahead due to their quartz material and their fork-shaped geometry compared to silicone cantilevers. The reason for this is explained by the fact that mechanical movement in QTF with two prongs, reducing the damping and dramatic decrement of high-quality factor even in the air.

Basically, the QTF consists of two forks which is coated with metal films. These forks vibrate under vacuum at a frequency of 32758 Hz, moving lateral when stimulated by alternating current excitation voltage [14, 42-51]. When hermetic casing of the QTFs were removed, resonance frequency of QTFs decreased due to air damping. This change not only affects the frequency but also changes the quality factor ( $Q_{vacuum} \approx 100,000$  and  $Q_{air} \approx 10,000$ ).

As mentioned, the working principle of QTF is similar to that of QCM. However, there are very few studies on its use in biosensors. The first and last use of QTF as a biosensor was performed by Su et al. (2002). In this study, anti-IgG was detected on polystyrene modified surfaces and the responses of the decorated surfaces against immunoglobulin G (IgG) were tested. As a result, it was found that the decorated QTF could work in the linear range of  $5\text{-}100\mu\text{g ml}^{-1}$ , but its reproducibility was low (% CV = 11% -16%). The reason of low reproducibility could be the nonhomogeneous polystyrene coating [52].

### 3. Surface Modification of Piezoelectric Crystals

Beside all advantages of both crystals in biosensor application, performance, reliability and stability of crystals have been directly affected from surface modification steps required for the functionalization and activation of the QCM and QTF surface, prior to bioreceptor immobilization. Therefore, to obtain highly sensitive and selective mass-sensitive biosensors for target analyte detection, surface modification of the QCM and QTF to create a recognition layer is crucial.

Plasma treatments can advantageously replace thermal, radiative, or chemical processes for the surface modification of materials. In fact, these treatments can be easily controlled and are environmentally friendly. Moreover, plasma modifies the surface layer at a depth from 50 to 500 Å, depending on power and time, leaves the bulk characteristic unaffected.

Plasma polymerized films are pinhole-free and highly cross-linked and therefore are insoluble, thermally stable, chemically inert and mechanically tough. Furthermore, such films are often highly coherent and adherent to a variety of substrates including conventional polymer, glass and metal surfaces. Depending upon the precursor that has been employed in plasma processing, the surface energy would be increased many times or the chemical structure could be converted into branched molecule groups to immobilize biological components such as antibody, enzyme, protein and etc.

#### 3.1 Surface Modification of Piezoelectric Crystals by Plasma Technology

Fourth state of matter, plasma, is composed of excited atoms, molecules, ions and radicals [53-54]. Plasma state occurs with the help of electrons generated by radio frequency (RF), microwave or hot filament discharge. This is a chaotic reactive chemical medium in which many plasma-surface reactions take place. Intense amounts of ions and excited species in the plasma can change the surface properties of even an inert material, ceramic [14, 53-54]. In addition, plasma techniques can successfully modify many complex materials [14, 53-55].

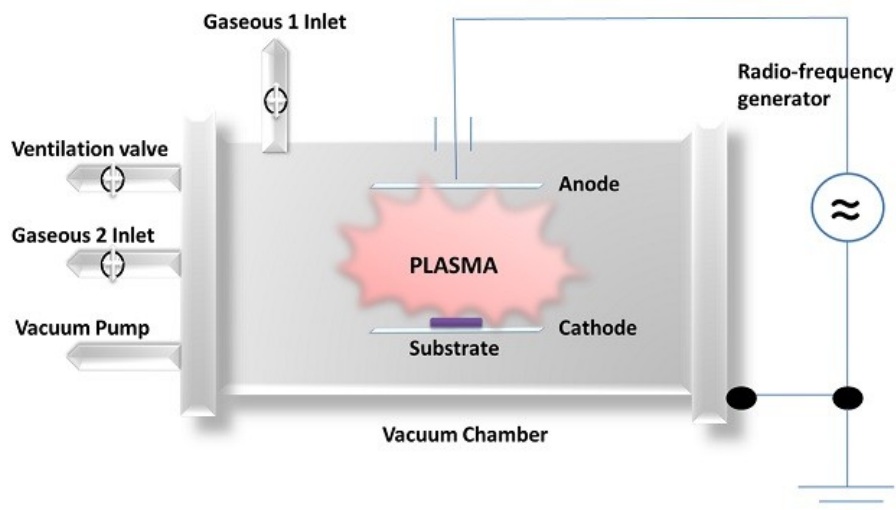


**Figure 1.** Schematic representation of the radio-frequency generated low-pressure plasma system.

Plasma techniques can make many changes such as changing the surface energy of the material, increasing the adhesion strength and biocompatibility. In addition, as a result of plasma modification, inexpensive thin films can be produced independent from the geometry of the material and structure of the material (metal, polymer, ceramic and / or composite). The most important advantage of this technique is that it is possible to change the chemical, electrical, optical, mechanical and biological structure of the material surface with high efficiency without affecting the bulk structure. This technique can be also used in the microelectronics industry for surface sterilization and cleaning, modification of the surface with a specific pattern in the case of masking [14, 53-54].

After plasma phase is formed with plasma technology, various changes can be made on the surface by plasma spraying, etching, cleaning, implantation and deposition [53]. Among them, plasma deposition has been mostly used in surface modification of mass sensitive biosensor. Plasma deposition method is preferred in many areas because the obtained coating may show completely different properties from the bulk. Inductively coupled plasma deposition, plasma-graft co-polymerization and plasma polymerization are techniques used to perform this method [14, 53-54]

In plasma polymerization method, polymer synthesis from monomer is achieved with the help of energetic electrons, ions and radicals found in chaotic plasma medium. Plasma polymerization is different compared to conventional polymerization methods because of the existence of both ions and radicals. Generally, the chemical composition of polymeric thin film produced by plasma polymerization differs from the polymer prepared by the conventional radical or ionic polymerization reaction. This difference is caused by the polymer formation mechanism. Plasma polymerization with plasma includes some steps like the formation of radicals from monomer by plasma activation, recombination of obtained radicals, and reactivation of recombinant molecules. Unlike the polymer synthesized by conventional polymerization reactions, the plasma polymer consists of repeating monomer units, highly cross-linked, fragmented and reordered complex units [14, 53-54].

#### 4. Applications of plasma modified QCM and QTF in Biomedical Applications

In the literature, plasma modified mass sensitive biosensors used in biomedical application have been presented for detecting genetically modified organism, human pathogen and mostly model protein, bovine serum albumin (BSA) over the past decade [14, 19, 29-32]. A DNA biosensor, which uses single-stranded DNA probe to detect human pathogen, *Vibrio parahaemolyticus*, based on a quartz crystal microbalance has been used. This single-stranded DNA probe was immobilized to QCM's surface by the help of functional groups formed by plasma polymerization of hexamethyldisilazane. After surface modification using plasma deposition, sensitivity of QCM increased to 86 ng/ml and linear range was found 86-468 ng/mL [29]. The other research was about the producing DNA biosensor to detect CaMV 35S promoter sequence (P35S) which is commonly inserted in the genome of the GMO regulating the transgene expression and the performance of the biosensor was evaluated with genomic DNAs of pflp gene-inserted transgenic tobacco plants. The immobilization was achieved with two different ways. These are chemisorption of thiolated probe on gold through thiol-gold interaction and covalent attachment of amines probe through glutaraldehyde activation. Amine probes were produced by ethylenediamine using plasma polymerization to produce amine probes on the quartz crystal surface. However, amine probes were not found efficient [30]. A study describing a new strategy to increase the performance of mass sensitive biosensor via electrospinning and plasma polymerization techniques was reported. Quartz crystal surface was firstly coated with polyvinyl alcohol nanofibers to increase surface to volume ratio. Then, nanofibers located on QCM were modified with allylamine monomer using plasma polymerization technique. The performance of modified QCM was tested with model protein, BSA and  $548 \pm 4$  Hz and  $50 \pm 5$  Hz frequency shifts were obtained for "dip and dry" method and "flow-cell method", respectively [19]. Our research group conducted a novel research to understand the effect of plasma-polymerized amine-rich thin films over QTF surfaces and to test their usability as a mass sensitive biosensor. Precursors, amylamine (amy), n-heptylamine (hep), or diaminocyclohexane (dach), were selected as a monomer for plasma polymerization technique and the performance of plasma modified QTF was studied by detecting model protein, BSA. According to detachment performance of thin films during glutaraldehyde activation, surfaces that produced by using amylamine was found optimum. After that, amylamine functionalized QTFs were tested with BSA ( $100\mu\text{g/mL}$ ) and resonance frequencies were decreased about 5 Hz [31]. At last, a QTF-based platform was produced by using a bi-layer film that coated by plasma-polymerized n-heptane (hep) and then by ethylenediamine (EDA), respectively in our laboratory. Then, the BSA detection performance of mass sensitive biosensor was tested and  $20 \pm 3.60$  Hz [32].

#### 5. Future Trends

In this chapter, biomedical application by plasma modified QCM and QTF-based mass sensitive biosensor is briefly summarized. Researches shown that plasma polymerization can be used for surface modification of piezoelectric crystals. The analysis with plasma polymerized crystals generally focused on the model protein, BSA, and etc. The plasma modified piezoelectric biosensors appear to be a suitable and convenient tool for detection of biomarkers. By virtue of this approach, it seems that both QCM and QTF will be favorable tool as a diagnosing disease. Future investigations can be focus on making systematic comparison between the performance of plasma modified-QCM and that of plasma modified-QTF.

## REFERENCES

- [1] Taleat, Z., Khoshroo, A., Mazloum-Ardakani, M. (2014). Screen-printed electrodes for biosensing: a review (2008–2013). *Microchimica Acta*, 181(9-10), 865-891.
- [2] Goode, J. A., Rushworth, J. V. H., Millner, P. A. (2014). Biosensor regeneration: a review of common techniques and outcomes. *Langmuir*, 31(23), 6267-6276.
- [3] Wang, J. (2006). Electrochemical biosensors: towards point-of-care cancer diagnostics. *Biosensors and Bioelectronics*, 21(10), 1887-1892.
- [4] Huet, A. C., Delahaut, P., Fodey, T., Haughey, S. A., Elliott, C., & Weigel, S. (2010). Advances in biosensor-based analysis for antimicrobial residues in foods. *TrAC Trends in Analytical Chemistry*, 29(11), 1281-1294.
- [5] Weller, M. G., Schuetz, A. J., Winklmaier, M., & Niessner, R. (1999). Highly parallel affinity sensor for the detection of environmental contaminants in water. *Analytica chimica acta*, 393(1-3), 29-41.
- [6] Mutlu, S., (2011). *Mass Sensitive Biosensors: Principles and Applications in Food* in: Mutlu M. (Ed.), *Biosensors in Food Processing, Safety, and Quality Control*. Taylor and Francis, CRC Press, New York, pp. 71-89.
- [7] Andreescu, S., Sadik, O. A. (2004). Trends and challenges in biochemical sensors for clinical and environmental monitoring. *Pure and applied chemistry*, 76(4), 861-878.
- [8] Alocilja, E. C. and Radke, S. M. (2003). Market analysis of biosensors for food safety. *Biosensors and Bioelectronics*, 18(5-6), 841-846.
- [9] Öztürk, K., Durusoy, M., Pişkin, E., 2008. *Journal of Bioactive and Compatible Polymers*. 26(6), 579-593.
- [10] Ricci, F., Volpe, G., Micheli, L., Palleschi, G. (2007). A review on novel developments and applications of immunosensors in food analysis. *Analytica chimica acta*, 605(2), 111-129.
- [11] Monošík, R., Stred'anský, M., Šturdík, E. (2012). Biosensors-classification, characterization and new trends. *Acta Chimica Slovaca*, 5(1), 109-120.
- [12] Kurosawa, S., Tawara, E., Kamo, N., Kobatake, Y. (1990). Oscillating frequency of piezoelectric quartz crystal in solutions. *Analytica Chimica Acta*, 230, 41-49.
- [13] Muratsugu, M., Ohta, F., Miya, Y., Hosokawa, T., Kurosawa, S., Kamo, N., Ikeda, H. (1993). Quartz crystal microbalance for the detection of microgram quantities of human serum albumin: relationship between the frequency change and the mass of protein adsorbed. *Analytical chemistry*, 65(20), 2933-2937.
- [14] Kaleli Can, G., *Development of QTF-Based Mass Sensitive Immunosensor for Phenylketonuria Diagnosis*. (TOBB University of Economics and Technology, ANKARA, 2018).
- [15] Alp, B., Mutlu, S., Mutlu, M. (2000). Glow-discharge-treated cellulose acetate (CA) membrane for a high linearity single-layer glucose electrode in the food industry. *Food Research International*, 33(2), 107-112.
- [16] Jenik, M., Seifner, A., Lieberzeit, P., Dickert, F. L. (2009). Pollen-imprinted polyurethanes for QCM allergen sensors. *Analytical and bioanalytical chemistry*, 394(2), 523-528.
- [17] Koshets, I. A., Kazantseva, Z. I., Shirshov, Y. M. (2003). Polymer films as sensitive coatings for quartz crystal microbalance sensors array. *Semiconductor Physics Quantum Electronics & Optoelectronics*.
- [18] Öztürk, K., Durusoy, M., Pişkin, E. (2008). A simple quartz crystal microbalance nucleic acid sensor for detection of telomerase. *Journal of Bioactive and Compatible Polymers*, 23(6), 579-593.

- [19] Rodoplu, D., Sen, Y., Mutlu, M. (2013). Modification of quartz crystal microbalance surfaces via electrospun nanofibers intended for biosensor applications. *Nanoscience and Nanotechnology Letters*, 5(4), 444-451.
- [20] Tsai, W. B., Chien, C. Y., Thissen, H., Lai, J. Y. (2011). Dopamine-assisted immobilization of poly (ethylene imine) based polymers for control of cell–surface interactions. *Acta biomaterialia*, 7(6), 2518-2525.
- [21] Zhang, C., Cappleman, B. P., Defibaugh-Chavez, M., Weinkauff, D. H. (2003). Glassy polymer-sorption phenomena measured with a quartz crystal microbalance technique. *Journal of Polymer Science Part B: Polymer Physics*, 41(18), 2109-2118.
- [22] Kabay, G., Can, G. K., & Mutlu, M. (2017). Amyloid-like protein nanofibrous membranes as a sensing layer infrastructure for the design of mass-sensitive biosensors. *Biosensors and Bioelectronics*, 97, 285-291.
- [23] Park, I. S., Kim, N. (1998). Thiolated Salmonella antibody immobilization onto the gold surface of piezoelectric quartz crystal. *Biosensors and Bioelectronics*, 13(10), 1091-1097.
- [24] Park, I. S., Kim, D. K., Adanyi, N., Varadi, M., Kim, N. (2004). Development of a direct-binding chloramphenicol sensor based on thiol or sulfide mediated self-assembled antibody monolayers. *Biosensors and Bioelectronics*, 19(7), 667-674.
- [25] Nakanishi, K., Muguruma, H., & Karube, I. (1996). A novel method of immobilizing antibodies on a quartz crystal microbalance using plasma-polymerized films for immunosensors. *Analytical chemistry*, 68(10), 1695-1700.
- [26] Mutlu, S., Saber, R., Koçum, C., Piskin, E. (1999). An immunosensor: Immobilization of anti-HBs antibody on glow-discharge treated piezoelectric quartz crystal for HBs-AG detection. *Analytical Letters*, 32(2), 317-334.
- [27] Wu, Z., Yan, Y., Shen, G., Yu, R. (2000). A novel approach of antibody immobilization based on n-butyl amine plasma-polymerized films for immunosensors. *Analytica chimica acta*, 412(1-2), 29-35.
- [28] JMutlu, S., Çökeliler, D., Shard, A., Goktas, H., Ozansoy, B., Mutlu, M. (2008). Preparation and characterization of ethylenediamine and cysteamine plasma polymerized films on piezoelectric quartz crystal surfaces for a biosensor. *Thin Solid Films*, 516(6), 1249-1255.
- [29] Chen, K. S., Chen, S. C., Lin, H. R., Yan, T. R., Tseng, C. C. (2007). A novel technique to immobilize DNA on surface of a quartz crystal microbalance by plasma treatment and graft polymerization. *Materials Science and Engineering: C*, 27(4), 716-724.
- [30] Karamollaoğlu, İ., Öktem, H. A., Mutlu, M. (2009). QCM-based DNA biosensor for detection of genetically modified organisms (GMOs). *Biochemical Engineering Journal*, 44(2-3), 142-150.
- [31] Can, G. K., Özgüzar, H. F., Kabay, G., Kömürcü, P., Mutlu, M. (2018). Simultaneous insulation and modification of quartz tuning fork surface by single-step plasma polymerization technique with amine-rich precursors. *MRS Communications*, 8(2), 541-549.
- [32] Özgüzar, H. F., Can, G. K., Kabay, G., Mutlu, M. (2019). Quartz tuning fork as a mass sensitive biosensor platform with a bi-layer film modification via plasma polymerization. *MRS Communications*, 1-9.
- [33] Akdoğan, E., Çökeliler, D., Marcinauskas, L., Valatkevicius, P., Valincius, V., Mutlu, M. (2006). A new method for immunosensor preparation: Atmospheric plasma torch. *Surface and Coatings Technology*, 201(6), 2540-2546.
- [34] Su, X., Chew, F. T., Li, S. F. (2000). Design and application of piezoelectric quartz crystal-based immunoassay. *Analytical Sciences*, 16(2), 107-114.
- [35] Richard, F. T., Jerome, S. S. (1996). *Handbook of Chemical and Biochemical Sensors*.

- [36] Ballantine Jr, D. S., White, R. M., Martin, S. J., Ricco, A. J., Zellers, E. T., Frye, G. C., Wohltjen, H. (1996). *Acoustic wave sensors: theory, design and physico-chemical applications*. Elsevier.
- [37] Janshoff, A., Galla, H. J., Steinem, C. (2000). Piezoelectric mass-sensing devices as biosensors—an alternative to optical biosensors?. *Angewandte Chemie International Edition*, 39(22), 4004-4032.
- [38] Lu, F., Lee, H. P., Lim, S. P. (2004). Quartz crystal microbalance with rigid mass partially attached on electrode surfaces. *Sensors and actuators A: Physical*, 112(2-3), 203-210.
- [39] Sauerbrey, G. Z. (1959). The use of quartz oscillators for weighing thin layers and for microweighing. *Z. Phys.*, 155, 206-222.
- [40] Bruckenstein, S., Shay, M. (1985). Experimental aspects of use of the quartz crystal microbalance in solution. *Electrochimica Acta*, 30(10), 1295-1300.
- [41] CKanazawa, K. K., Gordon, J. G. (1985). Frequency of a quartz microbalance in contact with liquid. *Analytical Chemistry*, 57(8), 1770-1771.
- [42] Castellanos-Gomez, A., Agraït, N., & Rubio-Bollinger, G. (2010). Carbon fibre tips for scanning probe microscopy based on quartz tuning fork force sensors. *Nanotechnology*, 21(14), 145702.
- [43] Heyde, M., Kulawik, M., Rust, H. P., & Freund, H. J. (2004). Double quartz tuning fork sensor for low temperature atomic force and scanning tunneling microscopy. *Review of scientific instruments*, 75(7), 2446-2450.
- [44] Labardi, M. (2007). Dynamic force microscopy with quartz tuning forks at high oscillation amplitudes. *Nanotechnology*, 18(8), 084019.
- [45] Song, S. H. (2009). Electrical characterization of a tuning fork crystal oscillator using dual-phase lock-in technique. *Review of Scientific Instruments*, 80(3), 034703.
- [46] Yang, C. H., Chang, T. H., Yang, M. J., Moore, W. J. (2002). A low noise transimpedance amplifier for cryogenically cooled quartz tuning fork force sensors. *Review of scientific instruments*, 73(7), 2713-2716.
- [47] Bettac, A., Koeble, J., Winkler, K., Uder, B., Maier, M., & Feltz, A. (2009). QPlus: atomic force microscopy on single-crystal insulators with small oscillation amplitudes at 5 K. *Nanotechnology*, 20(26), 264009.
- [48] Giessibl, F. J. (1998). High-speed force sensor for force microscopy and profilometry utilizing a quartz tuning fork. *Applied Physics Letters*, 73(26), 3956-3958.
- [49] Wastl, D. S., Weymouth, A. J., & Giessibl, F. J. (2013). Optimizing atomic resolution of force microscopy in ambient conditions. *Physical Review B*, 87(24), 245415.
- [50] Chen, Y., Li, Y., Shan, G., Zhang, Y., Wang, Z., Wang, M., Qian, J. (2018). Design and implementation of a novel horizontal AFM probe utilizing a quartz tuning fork. *International Journal of Precision Engineering and Manufacturing*, 19(1), 39-46.
- [51] Friedt, J. M., & Carry, E. (2007). Introduction to the quartz tuning fork. *American Journal of Physics*, 75(5), 415-422.
- [52] Zhang, J., Su, X. D., & O'shea, S. J. (2002). Antibody/antigen affinity behavior in liquid environment with electrical impedance analysis of quartz crystal microbalances. *Biophysical chemistry*, 99(1), 31-41.
- [53] Yasuda, H. (1984). Plasma polymerization for protective coatings and composite membranes. *Journal of membrane science*, 18, 273-284.
- [54] Kamińska, A., Kaczmarek, H., & Kowalonek, J. (2002). The influence of side groups and polarity of polymers on

the kind and effectiveness of their surface modification by air plasma action. *European Polymer Journal*, 38(9), 1915-1919.

[55] Mändl, S., & Rauschenbach, B. (2000). Plasma-Immersionen-Ionenimplantation. Ein neues Verfahren zur homogenen Oberflächenmodifizierung komplex geformter medizinischer Implantate-Plasma Immersion Ion Implantation. *New Technology for Homogeneous Modification of the Surface of Medical Implants of Complex Shapes. Biomedizinische Technik/Biomedical Engineering*, 45(7-8), 193-198.

# Altering Surface Topography of Electrospun Fibers

Murat Şimşek \*<sup>1</sup> 

## Abstract

When considering fiber-based materials, electrospinning is a fascinating method for producing polymeric nano/micro fibers in comparison with other techniques. Its wide range of applications from engineering to medicine make electrospinning gain great interest. Beside fibrous structure of fiber mats, topographical features on and/or inside fiber surfaces make them ideal candidates for site-specific applications. Several approaches have been adopted to gain desired topographical textures on individual fiber surfaces. Solvent properties, environmental conditions and also conditions for preparing fibers induce topographical changes in various physical characteristics.

## Keywords

Metal carbonyls; Surface Topography; Porous Fibers; Electrospinning; Humidity; Phase Separation.

<sup>1</sup>Inonu University, Biomedical Engineering, Malatya, Turkey

\*Corresponding Author: murat.simsek@inonu.edu.tr

Manuscript received date: May 24, 2019

Accept Date: June 26, 2019

Published Date: June 30, 2019.

## 1. INTRODUCTION

Electrospinning is a versatile technique that uses an external electric field to produce polymeric micro/nano sized fibers (Şimşek, 2018). Electrospinning includes the acceleration of a charged jet of polymer solution towards a grounded collector. The solvent evaporation and the stretching of the jet, caused by the repulsive forces of the charged molecules within the jet, are responsible for the formation of the polymer fibers. Electrospun micro and nanofibers have notable characteristics such as a large surface area to volume ratio, good pore interconnectivity, and high porosity. A further increase of the surface area by incorporating tailored surface topographies is therefore of major interest for many applications including tissue engineering, drug delivery, catalysis, filtration and sensors (Baker et al., 2015; Chen and Tung, 2017; D. Li and Xia, 2004; Liu et al., 2015; J. Yu et al., 2008). For example, porosity in electrospun polymer fibers has great advantageous for tissue engineering. The porous surface of nano or micro structure is not only important for an increase in cell attachment and tissue compatibility but also prerequisite for the transport of oxygen and nutrient supply to the cells and for the cellular growth. Porous nanofibers can be obtained by selecting particular solvents or solvent mixtures, polymer mixtures, optimizing electrospinning conditions and/or controlling environmental conditions.

In the presented review, several mechanisms involved in the production of electrospun fibers having various topographical textures are identified in the presence of literature.

## 2. MECHANISMS

A number of methods have been adopted to prepare electrospun nanofibers at various surface characteristics. The following subsections were organized as based on their mechanisms that induce surface textures on electrospun fibers in different manner.

### 2.1 Breath figures

The breath figures mechanism was firstly observed by Srinivasarao et al. (Srinivasarao, Collings, Philips, and Patel, 2001), who described the formation of pores on a polystyrene (PS) film in a humid environment. In that case the solvent evaporation causes a lowering of the temperature on the surface of the film. Water vapor from the atmosphere is condensed on the surface, the resulting water condensation begins with the nucleation of droplets in random positions followed by coalescence and potential organization to minimize thermodynamic energy (Marcos-Martin, Beysens, Bouchaud, Godrèche, and Yekutieli, 1995). Finally, the pores were created by the evaporation of the water molecules from the surface (Figure 1 a). The use of humidity to increase

the porosity of electrospun fibers has also been proposed by other researchers (Casper, Stephens, Tassi, Chase, and Rabolt, 2004; Nezarati, Eifert, and Cosgriff-Hernandez, 2013).

Breath figures are nano-to micron- sized patterned arrays of defects. However, the pores formed on electrospun fibers are not uniform and this may be due to the dynamic condition of the electrospinning jet as compared to the static conditions where the effects of breath figures are dominant in thin films (Ramakrishna). In addition, this process is relatively slower compared with phase separation and only forms pores on the surface of electrospun nanofibers (Lu and Xia, 2013). Nevertheless, porous nanofibers can be obtained by electrospinning of a kind of hydrophobic polymer from a volatile and water-compatible solvent at a proper level of relative humidity.

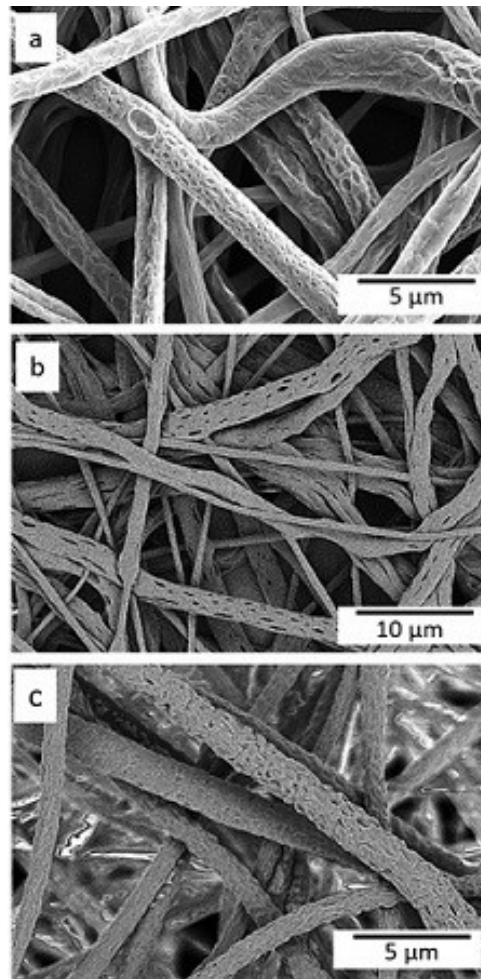


**Figure 1.** PCL fiber surfaces with a) breath figures, b) pores and c) rough

## 2.2 Non-solvent induced phase separation (NIPS)

There are two kinds of NIPS processes. The first one is also known as immersion precipitation method by which a cast polymer solution is immersed in a nonsolvent bath to initiate phase separation (D.-J. Lin, Chang, Chen, Lee, and Cheng, 2006). The other one is based on mixing solvent and non-solvent having higher boiling point than that of solvent with an appropriate amount that does not cause phase separation before electrospinning. In immersion precipitation, the polymer precipitates rapidly after immersion in a non-solvent bath resulting in highly porous structures. A simple and efficient method to induce porosity both in the core and on the surface of electrospun fibers were demonstrated (Nayani et al., 2012). Porous fibers were obtained for poly(acrylonitrile) (PAN)/dimethyl formamide (DMF), PS/DMF, PS/toluene, and poly(methyl methacrylate)/DMF polymer/solvent systems when using non-solvent water bath as collector. Authors concluded that water and DMF have excellent miscibility which favored the generation of porosity by NIPS. Apart from that nearly smooth fibers having no surface porosity were obtained when hexane was used as the nonsolvent bath. In the case where solvent and non-solvent are used, the composition changes and falls into the phase separation region because of the different volatility between solvent and nonsolvent. Thus, porous structures can be created during the subsequent solidification process of electrospinning (Katsogiannis, Vladislavljević, and Georgiadou, 2015; Lubasova and Martinova, 2011; Qi, Yu, Chen, and Zhu, 2009; Wei et al., 2013) (Figure

1 b). The presence of a non-solvent can induce thermodynamic instability of the solution and initiates the phase separation process. An advantage of NIPS over the other phase separation mechanisms is that it can be controlled and can provide reproducible results.

PS fibers with micro- and nano-porous structures both in the core and/or on the fiber surfaces were electrospun by varying solvent compositions and solution concentrations of the PS solutions (J. Lin, Ding, and Yu, 2010). According to the authors the tetrahydrofuran (THF)/DMF mixing ratio in PS solutions was proved to be the key parameter to affect porous structure. In the process, the phase separation resulted from rapid evaporation of solvent in electrospinning. The high vapor pressure solvent THF created the fibers comprising nanoporous sheaths with 3D interconnected nanofibrils cores. As the vapor pressure of the solvent mixtures decreased, the micro and nanoporous structures on the fiber surfaces disappeared but wrinkled or smooth surfaces presented. The fibrous mats electrospun from 1/3 THF/DMF solvent system showed largest specific surface area and pore volume. In a study by Byong-Taek et al. (Nguyen, Bao, Park, and Lee, 2013), fibrous scaffolds composed of electrospun porous poly( $\epsilon$ -caprolactone) (PCL) fibers were produced for bone tissue engineering. In this study, various ratios of dichloromethane (DCM)/Acetone (ACT) (10/0, 8/2, 6/4 and 5/5, v/v) solvents were used to dissolve PCL, which could affect the surface structure of the fibers. When only DCM was used, the morphology of the PCL fiber surface was rough. However, when DCM/ACT (50/50) solvent was used, the PCL fibers were more porous with many pores with size distribution in the range of 500–1000 nm. *In vitro* and *in vivo* results verified that porous PCL fiber-based fibrous scaffolds after 12 h of immersion in simulated body fluid was excellent for cell interaction, growth, proliferation and enabled greater acceleration of bone formation than other samples. According to a study by Tung and Chen (Chen and Tung, 2017), the pore size of PS fibers increased with increasing dimethyl sulfoxide (DMSO) fraction, indicating that the nonsolvent must play an important role in the formation of the pores. Moreover, the shape and orientation of the pores are affected by the stretching forces. The porous structure imparted superhydrophobic surface to the fibrous mats, and thus the fibers could selectively adsorb oils while repelled water. Georgiadou et al. (Katsogiannis et al., 2015) concluded that the pore formation was favored at high good/poor solvent ratios. In their study, the effect of the solvent properties on the size and surface morphology of electrospun PCL fibers was investigated. Chloroform (CF), DCM, THF and formic acid (FA) were used as good solvents in mixtures with a poor solvent, DMSO, in order to generate pores on PCL fiber surface. The production of porous, bead free fibers was achieved using 12.5% w/v PCL in CF/DMSO solution with good/poor solvent ratios varying from 75% to 90% v/v. However, DCM and THF were proven to be less suitable good solvents for the process due to the formation of a solid skin on the jet surface, caused by the limited diffusivity of the polymer molecules from the jet surface to the liquid core and its subsequent collapse. FA was found to be unsuitable due to its similar evaporation rate to DMSO. The production of fibers with ribbon cross sections or fibers with beads was more pronounced at low good/poor solvent ratios. In another investigation, reproducible buckled and porous sub-micron diameter electrospun PCL fibers were produced by simple electrospinning process for biomedical applications (Luwang Laiva et al., 2014). PCL solutions were prepared with in the binary solvent combinations (with different vapor pressures) of CF with ethanol, DCM, DMF, DMSO, ethyl acetate and diethyl ether a ratio of 9:1 v/v respectively, to make a 16% (w/v) solution for electrospinning. Fiber morphologies was affected with various degree by solvent combinations used for the fabrication of sub-micron fibers. The results suggested that the solution viscosity, the collecting distance and the type of solvent combination used could be an optimum parameter for the generation of porous-buckled fibers with narrow pore size distribution. Georgiadou et al. (Katsogiannis, Vladislavljević, and Georgiadou, 2016) also confirmed that electrospinning process parameters had an effect on surface morphology of porous electrospun fibers which was obtained by using PCL solution in a binary solvent mixture of 90/10 %v/v CF/ DMSO. In another study, PAN porous fibers were spun in one step by electrospinning a ternary system of PAN/DMF/water (X. Yu et al., 2010). The spinodal decomposition phase separation resulted in the porous structure. Fortunato et al. (Yazgan et al., 2017) confirmed that irregular and interconnected surface topographies was obtained on PCL fibers by using CF/DMSO solvent system beginning of 35% RH. Megelski et al. (Megelski, Stephens, Chase, and Rabolt, 2002) observed that the ratio of the less volatile DMF increased in THF/DMF solvent mixtures, therefore reducing the vapor pressure, surface roughness or microtexture was observed of PS fibers. The microtexture finally disappeared, leaving a smooth surface with decreasing solvent volatility by using 100% DMF.

### 2.3 Vapor induced phase separation (VIPS)

In the VIPS method, vapors (usually water) are condensed as nonsolvents that cause originally homogeneous solutions to phase separate and porous structures can be obtained after the removal of solvents (C.-L. Li et al., 2010; Srinivasarao et al., 2001). VIPS also occurs in the electrospinning process (Figure 1 c). Solvent evaporation cools down the jet surface and the moisture condense from the atmosphere. Initiating of the nucleation and growth of the water-rich phase floating on the solution subsequently leaves pores on the fiber surface (Lu and Xia, 2013; Megelski et al., 2002; Nezarati et al., 2013; Park and Lee, 2010; Wu et al., 2012).

Many researches highlighted that the effects of relative humidity on electrospun fiber morphology are dependent on polymer hydrophobicity, solvent miscibility with water, and solvent volatility (Nezarati et al., 2013). Three polymers (poly(ethylene

glycol) (PEG), PCL, and poly(carbonate urethane) (PCU) were electrospun at a range of relative humidities (RH = 5%-75%). At high relative humidity (>50%), three distinct effects were observed based on individual polymer properties. An increase in fiber breakage and loss of fiber morphology occurred in the PEG system as a result of increased water absorption at high relative humidity. In contrast, surface pores on PCL fibers were observed and hypothesized to have formed via VIPS. Finally, decreased PCU fiber collection occurred at high humidity likely due to increased electrostatic discharge. It was demonstrated that the amount of moisture in the air affected the surface morphology of electrospun PS fibers from THF (Casper et al., 2004). Electrospinning in an atmosphere of less than 25% humidity produced smooth fibers without any surface features. When the humidity was above 30%, pores began to form on the surface of the fiber. Increasing the amount of humidity caused an increase in the number of pores on the surface, the pore diameter, and the pore size distribution. In addition to that higher molecular weight solutions caused fibers to contain larger pores that were less uniform in shape and size. Three solvent systems (i.e., DMF, THF, and DMF - THF mixture) were tested under four controlled levels of relative humidity (Lu and Xia, 2013). Whereas only solid PS fibers with smooth surfaces were produced at low relative humidity (2%), both internally and externally porous PS fibers/yarns were obtained by conducting electrospinning at high relative humidity (22%, 42%, and 62%). Furthermore, it was discovered that the low vapor pressure of DMF facilitated the formation of internal porosity while the high vapor pressure of THF hindered the formation of interior pores and could only produce surface porosity. Megelski et al. (Megelski et al., 2002) proved that increasing relative humidity from 20 to 50% would increase the pore formation for the fibers from PS/THF polymer/solvent system.

#### 2.4 Thermally induced phase separation (TIPS)

In the TIPS method, a homogeneous polymer solution is first prepared at an elevated temperature and then rapidly cooled to a temperature where the solvent quality turn to be poor to polymer and phase separation occurs (Chang, Beltsios, Chen, Lin, and Cheng, 2014). This method can be applied to produce electrospinning porous polymer fibers by controlling the collector at relatively low temperature to induce phase separation (McCann, Marquez, and Xia, 2006). This method needs post-treatments to remove residual solvents because the fibers are not completely dried in the electrospinning process.

McCann et al. (McCann et al., 2006) exploited the role of TIPS in the creation of highly porous electrospun nanofibers by using a liquid nitrogen bath as the quenching medium. The fibers were frozen in the liquid nitrogen bath resulting in TIPS. It was noted that the distance between the metallic needle and the collector should be chosen properly to ensure that the solvent could not be completely evaporated before the jet reached the liquid nitrogen. Lee et al. (J. F. Kim, Kim, Lee, and Drioli, 2016) reviewed TIPS and electrospinning methods for preparation of fluoropolymer membranes, particularly for the polyvinylidene fluoride and polyethylene chlorotrifluoroethylene membranes. They focused on controlling the membrane morphology from the thermodynamic and kinetic perspectives to understand the relationship between the membrane morphology and fabrication parameters. It was reported that by immersing the collector in a bath of liquid nitrogen, porous PS fibers can be obtained through TIPS between the solvent-rich and solvent-poor regions in the fiber during electrospinning (McCann et al., 2006). Isotactic polypropylene and poly(vinylidene fluoride) porous fibers were successfully prepared as two of the most commonly used membrane materials by electrospinning at 200 °C combined with TIPS (Ye, Lin, Huang, Liang, and Xu, 2013). The as-spun porous fibers have high porosity and more than a 100-fold increase in specific surface area compared with non-porous fibers, which would dramatically improve their in-service performance as separation media.

#### 2.5 Another approaches

Porous nanofibers could be prepared by the selective removal of a component from nanofibers made of composite or blended materials. For example, the structural changes for fibers consisting of a PLA/polyvinylpyrrolidone (PVP) blend were investigated when one of the two components was selectively removed from the composites (Bognitzki et al., 2001). It was found that porous nanofibers were obtained after selective removal of PVP by water extraction or alternatively to remove PLA by annealing at elevated temperatures, when equal amount of the two polymers were loaded into the electrospinning solution. A leaching treatment from bi-continuous material of gelatin/PCL nanofibers lead to the formation of novel 3D porous nanofibers with reduced fiber diameter (Zhang, Feng, Huang, Ramakrishna, and Lim, 2006). The fiber surface after leaching treatment became rough and irregular because of the existence of many interconnected striated ridges, grooves and ellipsoidal shaped pores with the long axis oriented in the direction of the fiber axis. Gupta et al. (Gupta et al., 2009) produced porous nylon-6 fibers from the Lewis acid base complication of gallium trichloride (GaCl<sub>3</sub>) and nylon-6 using electrospinning, followed by GaCl<sub>3</sub> removal. In another study, highly porous fibers were prepared by water-bath electrospinning from PCL, and its blends with methoxy poly(ethylene glycol) (MPEG) as potential tissue scaffold material (Pant et al., 2011). A new approach was reported to fabricate electrospun polymer nonwoven mats with porous surface morphology by varying the collector temperature during electrospinning (C. H. Kim et al., 2006). Polymers such as poly(L-lactide), PS, and poly(vinyl acetate) were dissolved in volatile solvents, DCM and THF, and subjected to electrospinning. The temperature of the collector in the electrospinning device was varied by a heating system. According to the results the surface morphology, porous structure, and the properties such as pore size, depth, shape, and distribution of the nonwoven mats were greatly influenced by the collector temperature. In a

study, inter-surface-connected porous fibers based on rapid phase separation between poly(propylene carbonate) and PCL were produced (Wang et al., 2015). ADCs cultured on electrospun fibers with intersurface-connected pores showed increased cellular adhesion, proliferation and differentiation than those cultured on the fiber with blind-holes. In another study, the morphology, structure and tensile properties of PLA porous nanofibers were studied (Y. Li, Lim, and Kotaki, 2015). Different crystallization ability of PLA was electrospun from mixed solvent of DCM and DMF into porous nanofibers through two kinds of spinnerets (nozzle and channel spinnerets) in a highly humid environment. Results showed that take-up velocity affected the porous morphology of nanofibers, which was more obvious in the case of channel-based spinneret and PLA with low crystallization ability. In the case of PLA with high crystallization ability, an increase in take-up velocity led to more highly packed internal structure, which could contribute to the enhancement in tensile properties. In addition, tensile properties of porous nanofibers of PLA with low crystallization ability could be manipulated by surface morphology control via channel-based electrospinning system.

Many researchers have also verified that electrospinning parameters, including molecular weight of polymer (Casper et al., 2004), polymer concentration (Kongkhleng et al., 2008; J. Lin et al., 2010), solvent (Kongkhleng et al., 2008; J. Lin et al., 2010), spinning voltage (Kongkhleng et al., 2008), had an influence on morphology of porous nanofiber in terms of nanoporosity as well as size, shape, and distribution of these pores.

### 3. CONCLUSION

Porous materials have found widespread use in a wide variety of applications such as filtration, catalysis, and biomedical research. Through rational design and controlled fabrication, it is possible to obtain desired porous fibers at different characteristics. Since different mechanisms resulting from relative humidity, solvent and polymer properties and also electrospinning conditions involves in the processing, it essential to carefully design experimental setup for various applications.

### REFERENCES

- Baker, B. M., Trappmann, B., Wang, W. Y., Sakar, M. S., Kim, I. L., Shenoy, V. B., . . . Chen, C. S. (2015). Cell-mediated fibre recruitment drives extracellular matrix mechanosensing in engineered fibrillar microenvironments. *Nature materials*, 14(12), 1262-1268.
- Bognitzki, M., Frese, T., Steinhart, M., Greiner, A., Wendorff, J. H., Schaper, A., and Hellwig, M. (2001). Preparation of fibers with nanoscaled morphologies: Electrospinning of polymer blends. *Polymer Engineering and Science*, 41(6), 982-989.
- Casper, C. L., Stephens, J. S., Tassi, N. G., Chase, D. B., and Rabolt, J. F. (2004). Controlling Surface Morphology of Electrospun Polystyrene Fibers: Effect of Humidity and Molecular Weight in the Electrospinning Process. *Macromolecules*, 37(2), 573-578.
- Chang, H.-H., Beltsios, K., Chen, Y.-H., Lin, D.-J., and Cheng, L.-P. (2014). Effects of cooling temperature and aging treatment on the morphology of nano- and micro-porous poly(ethylene-co-vinyl alcohol) membranes by thermal induced phase separation method. *Journal of Applied Polymer Science*, 131(12).
- Chen, P.-Y., and Tung, S.-H. (2017). One-Step Electrospinning To Produce Nonsolvent-Induced Macroporous Fibers with Ultrahigh Oil Adsorption Capability. *Macromolecules*, 50(6), 2528-2534.
- Gupta, A., Saquing, C. D., Afshari, M., Tonelli, A. E., Khan, S. A., and Kotek, R. (2009). Porous Nylon-6 Fibers via a Novel Salt-Induced Electrospinning Method. *Macromolecules*, 42(3), 709-715.
- Katsogiannis, K. A. G., Vladisavljević, G. T., and Georgiadou, S. (2015). Porous electrospun polycaprolactone (PCL) fibres by phase separation. *European Polymer Journal*, 69, 284-295.
- Katsogiannis, K. A. G., Vladisavljević, G. T., and Georgiadou, S. (2016). Porous electrospun polycaprolactone fibers: Effect of process parameters. *Journal of Polymer Science Part B: Polymer Physics*, 54(18), 1878-1888.
- Kim, C. H., Jung, Y. H., Kim, H. Y., Lee, D. R., Dharmaraj, N., and Choi, K. E. J. M. R. (2006). Effect of collector temperature on the porous structure of electrospun fibers. *Macromolecular Research*, 14(1), 59-65.
- Kim, J. F., Kim, J. H., Lee, Y. M., and Drioli, E. (2016). Thermally induced phase separation and electrospinning methods for

emerging membrane applications: A review. *Advances in Materials. Separations: Materials, Devices and Processes*, 62(2), 461-490.

Kongkhleng, T., Kotaki, M., Kousaka, Y., Umemura, T., Nakaya, D., and Chirachanchai, S. (2008). Electrospun Polyoxymethylene: Spinning Conditions and Its Consequent Nanoporous Nanofiber. *Macromolecules*, 41(13), 4746-4752.

Li, C.-L., Wang, D.-M., Deratani, A., Quémener, D., Bouyer, D., and Lai, J.-Y. (2010). Insight into the preparation of poly(vinylidene fluoride) membranes by vapor-induced phase separation. *Journal of Membrane Science*, 361(1), 154-166.

Li, D., and Xia, Y. (2004). Electrospinning of Nanofibers: Reinventing the Wheel? *Advanced Materials*, 16(14), 1151-1170.

Li, Y., Lim, C. T., and Kotaki, M. (2015). Study on structural and mechanical properties of porous PLA nanofibers electrospun by channel-based electrospinning system. *Polymer*, 56, 572-580.

Lin, D.-J., Chang, H.-H., Chen, T.-C., Lee, Y.-C., and Cheng, L.-P. (2006). Formation of porous poly(vinylidene fluoride) membranes with symmetric or asymmetric morphology by immersion precipitation in the water/TEP/PVDF system. *European Polymer Journal*, 42(7), 1581-1594.

Lin, J., Ding, B., and Yu, J. (2010). Direct fabrication of highly nanoporous polystyrene fibers via electrospinning. *ACS Appl Mater Interfaces*, 2(2), 521-528.

Liu, C., Hsu, P.-C., Lee, H.-W., Ye, M., Zheng, G., Liu, N., . . . Cui, Y. (2015). Transparent air filter for high-efficiency PM2.5 capture. *Nature Communications*, 6, 6205.

Lu, P., and Xia, Y. (2013). Maneuvering the internal porosity and surface morphology of electrospun polystyrene yarns by controlling the solvent and relative humidity. *Langmuir*, 29(23), 7070-7078.

Lubasova, D., and Martinova, L. (2011). Controlled Morphology of Porous Polyvinyl Butyral Nanofibers. *Journal of Nanomaterials*. 2011, 6.

Luwang Laiva, A., Venugopal, J. R., Sridhar, S., Rangarajan, B., Navaneethan, B., and Ramakrishna, S. (2014). Novel and simple methodology to fabricate porous and buckled fibrous structures for biomedical applications. *Polymer*, 55(22), 5837-5842.

Marcos-Martin, M., Beysens, D., Bouchaud, J. P., Godrèche, C., and Yekutieli, I. (1995). Self-diffusion and 'visited' surface in the droplet condensation problem (breath figures). *Physica A: Statistical Mechanics and its Applications*, 214(3), 396-412.

McCann, J. T., Marquez, M., and Xia, Y. (2006). Highly Porous Fibers by Electrospinning into a Cryogenic Liquid. *Journal of the American Chemical Society*, 128(5), 1436-1437.

Megelski, S., Stephens, J. S., Chase, D. B., and Rabolt, J. F. (2002). Micro- and Nanostructured Surface Morphology on Electrospun Polymer Fibers. *Macromolecules*, 35(22), 8456-8466.

Nayani, K., Katepalli, H., Sharma, C. S., Sharma, A., Patil, S., and Venkataraghavan, R. (2012). Electrospinning Combined with Nonsolvent-Induced Phase Separation To Fabricate Highly Porous and Hollow Submicrometer Polymer Fibers. *Industrial and Engineering Chemistry Research*, 51(4), 1761-1766.

Nezarati, R. M., Eifert, M. B., and Cosgriff-Hernandez, E. (2013). Effects of humidity and solution viscosity on electrospun fiber morphology. *Tissue Engineering Part C Methods*, 19(10), 810-819.

Nguyen, T.-H., Bao, T. Q., Park, I., and Lee, B.-T. (2013). A novel fibrous scaffold composed of electrospun porous poly( $\epsilon$ -caprolactone) fibers for bone tissue engineering. *Journal of Biomaterials Applications*, 28(4), 514-528.

- Pant, H. R., Neupane, M. P., Pant, B., Panthi, G., Oh, H. J., Lee, M. H., and Kim, H. Y. (2011). Fabrication of highly porous poly (varepsilon-caprolactone) fibers for novel tissue scaffold via water-bath electrospinning. *Colloids and Surfaces B: Biointerfaces*, 88(2), 587-592.
- Park, J. Y., and Lee, I. H. (2010). Relative humidity effect on the preparation of porous electrospun polystyrene fibers. *J Nanosci Nanotechnol*, 10(5), 3473-3477.
- Qi, Z., Yu, H., Chen, Y., and Zhu, M. (2009). Highly porous fibers prepared by electrospinning a ternary system of nonsolvent/solvent/poly(l-lactic acid). *Materials Letters*, 63(3), 415-418.
- Ramakrishna, S. A. F., Kazutoshi Teo, Wee-Eong Lim, Teik-Cheng Ma, Zuwei. *An Introduction to Electrospinning and Nanofibers*.
- Srinivasarao, M., Collings, D., Philips, A., and Patel, S. (2001). Three-Dimensionally Ordered Array of Air Bubbles in a Polymer Film. *Science*, 292(5514), 79-83.
- Şimşek, M. (2018). *Fabrication of Fibrous Tissue Scaffolds*. Dubai: GlobeEdit.
- Wang, Y., Deng, J., Fan, R., Tong, A., Zhang, X., Zhou, L., . . . Guo, G. (2015). Novel nanoscale topography on poly(propylene carbonate)/poly(ε-caprolactone) electrospun nanofibers modifies osteogenic capacity of ADCs. *RSC Advances*, 5(101), 82834-82844.
- Wei, Z., Zhang, Q., Wang, L., Wang, X., Long, S., Yang, J. J. C., and Science, P. (2013). Porous electrospun ultrafine fibers via a liquid–liquid phase separation method. *Colloid and Polymer Science*, 291(5), 1293-1296.
- Wu, J., Wang, N., Wang, L., Dong, H., Zhao, Y., and Jiang, L. (2012). Electrospun Porous Structure Fibrous Film with High Oil Adsorption Capacity. *ACS Appl Mater Interfaces*, 4(6), 3207-3212.
- Yazgan, G., Dmitriev, R. I., Tyagi, V., Jenkins, J., Rotaru, G.-M., Rottmar, M., . . . Fortunato, G. (2017). Steering surface topographies of electrospun fibers: understanding the mechanisms. *Scientific Reports*, 7(1), 158.
- Ye, X.-Y., Lin, F.-W., Huang, X.-J., Liang, H.-Q., and Xu, Z.-K. (2013). Polymer fibers with hierarchically porous structure: combination of high temperature electrospinning and thermally induced phase separation. *RSC Advances*, 3(33), 13851-13858.
- Yu, J., Qiu, Y., Zha, X., Yu, M., Yu, J., Rafique, J., and Yin, J. (2008). Production of aligned helical polymer nanofibers by electrospinning. *European Polymer Journal*, 44(9), 2838-2844.
- Yu, X., Xiang, H., Long, Y., Zhao, N., Zhang, X., and Xu, J. (2010). Preparation of porous polyacrylonitrile fibers by electrospinning a ternary system of PAN/DMF/H<sub>2</sub>O. *Materials Letters*, 64(22), 2407-2409.
- Zhang, Y. Z., Feng, Y., Huang, Z. M., Ramakrishna, S., and Lim, C. T. (2006). Fabrication of porous electrospun nanofibres. *Nanotechnology*, 17(3), 901-908.

# Biochips for Physical Exercise Studies

Neşe Akpınar Kocakulak <sup>\*1</sup>, İbrahim Ünal<sup>2</sup>

## Abstract

In early 1990s, microfluidics technology was mainly aiming at the manipulation of fluids in micro-scale and nanoscale. At present, with the development of microfluidics, it has been widely used in the life science and medical researches with significant achievements. The microfluidics technology can be used in single cell capture, cell screening, and synthesis of biomacromolecules. Some microfluidic chips have already been commercialized and applied in disease detection, drug delivery and bioscience. However, the physical index oriented wearable technology ignored another part of the most important indications in health monitoring i.e. the body fluid. The body fluid in this review refers to the blood, sweat, interstitial fluid, saliva, tears, and urine. The current medical procedures for the testing of body fluid involve using highly sophisticated instrument such as atomic absorption spectrometry, ion chromatography and gas chromatograph for the detection of specific targets in body fluid. For correct detection of changes in body fluids, it is necessary to intervene in body fluids naturally. Physical fatigue is known to have a direct effect on body fluids. For this reason, microfluidic chips are used in experiments after exercise. Also exercise; diabetes, cancer, cardiovascular disease, muscle, immune, and age-related decline in cognitive function have been documented against the protect. In addition, regular physical exercise is the most powerful initiative known to have positive effects on health and aging.

## Keywords

Microfluidics devices; microfabrication; microfluidics; microchips; biochips.

<sup>1</sup>Izmir Democracy University, Faculty of Health Sciences, Department of Sports Sciences

<sup>2</sup>Izmir Democracy University, Institute of Sciences, Department of Biomedical Sciences and Engineering

\*Corresponding Author: nese.kocakulak@idu.edu.tr

Manuscript received date: June 14, 2019

Accept Date: June 28, 2019

Published Date: June 30, 2019.

## 1. INTRODUCTION

Miniaturization is one of the key driving factors in the evolution of modern technology [1, 2]. It enables devices to have complex functionalities in a smaller volume, with less energy consumption and lower costs per implemented function. Other correlated benefits from miniaturization include faster processing time, lower manufacturing and operational costs, smaller volumes of needed samples and reactants, integration with other devices (multifunctionality), increased safety and reliability by having less external interconnects between the different parts, and high throughput [3]. Miniaturization brings molecules or samples closer together for more effective, efficient, and rapid interactions [4]. Miniaturization also increases the portability of microfluidic devices because the devices are compact yet fully functional by themselves [4].

Microfluidics allows for handling of fluid with volumes typically in the range of nano- to microliters ( $10^{-9}$  to  $10^{-6}$  L) or smaller [3, 4]. The attractive and advantageous characteristics of microfluidics include down-scaling and miniaturization. Microfluidics utilizes and consumes less fluid volumes, and requires fewer materials to make the actual device, making the device and procedures more cost-effective and capable of being mass produced [5, 6]. The downsizing of microfluidic channels results in faster analysis and response times, owing to higher surface to volume ratios, shorter diffusion distances, and smaller heating capacities [4].

Several new microsystems have been created by the fabrication and integration of small electrical and mechanical components put together as a system, using techniques that are inherited from or related to the integrated circuit technologies (IC) [7]. On of these, microelectromechanical systems (MEMS) are precise, miniaturized systems with primary functionalities in both electrical and mechanical domains, with applications covering a large range of phenomena in the physical, chemical, and biological domains [3]. MEMS devices open the possibility of cointegration in a single complex system of functions like sensing, electronic signal processing, and electromechanical actuation that are traditionally performed by distinctly separated

and bulky functional blocks. Depending on the specific domain of functionality and application of these devices, different terms have been coined to categorize them. As examples, RF MEMS devices are used for radio frequency telecommunication applications (e.g., switches, transmission lines, and antennas) [8], optical MEMS refers to devices interacting with light (e.g., image scanner micro mirrors, and optical switches) [9, 10] and bio-MEMS [11]/microfluidics [12] are used in systems applied to biological assays and fluid manipulation (e.g., body fluids and cell manipulation, DNA analysis [13], toxins detection, diseases diagnosis and treatment, and drug delivery [14]).

The experience accumulated for the microfluidic chips in the life science and medical research recently opened a new gate for the wearable technology, i.e. wearable microfluidics [15, 16]. As an emerging technology of life science, electronics, material science and chemistry, wearable technology has experienced a significant development over the past few years. Wearable technology has been extensively used in life monitoring [17, 18], disease detection [19, 20], sports science [21, 22] and military [23], etc. Wearable technology refers to the certain kind of equipment that can be directly wore or integrated in the cloths and accessories. Traditional wearable technology aimed at detection of physical index such as heart rate [24], body temperature [25], motion tracking [26], bioelectricity signal [27] and steps [28] using photoelectric detection method [29].

### 1.1 Microfabrication

The fabrication of small scale microfluidic devices relies on high-precision micromachining techniques capable of creating high aspect ratio structures. Micromachining techniques can be basically divided in two major categories: bulk and surface techniques. Bulk techniques rely on the direct modification of a substrate material, usually a monocrystalline silicon wafer, glass, quartz or thick polymer matrix, used as a basic (bulk) material or support to shape the desired structures. Typical substrate thicknesses are in the range of several tens to hundreds of micrometers (Fig. 1 A). On the other hand, surface micromachining techniques involve the deposition of various layers of materials in the form of thin films and their definition into the desired structural shape (Fig. 1 B). Typical thicknesses of the various layers in surface micromachining techniques are in the range of a few nanometers to a few micrometers, much smaller than the bulk thickness, which is used to support the microfluidic device itself [3].

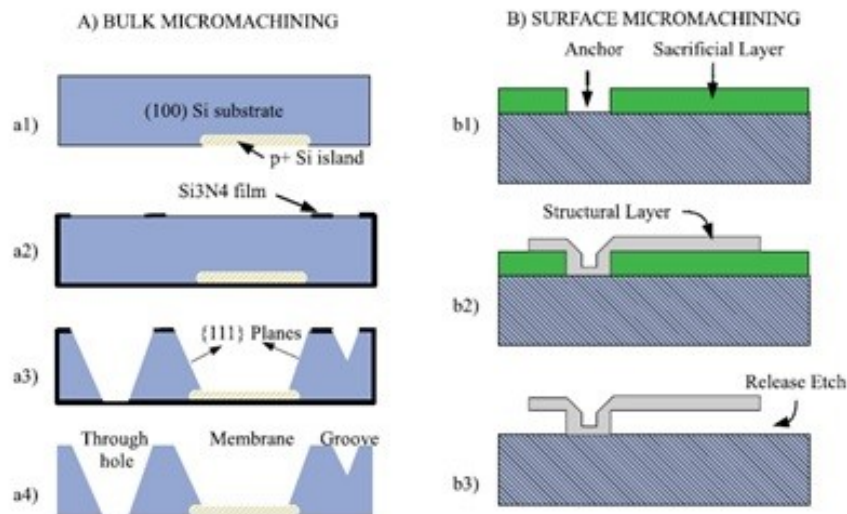


**Figure 1.** Schematic illustration examples of (a) bulk micromachining process in a silicon substrate and (b) surface micromachining process [3].

### 1.2 Microfluidics devices

These devices are of great interest in physical, chemical, and biological applications. They have stringent specifications in terms of the precision involved in their fabrication as well as in terms of the compatibility between the different materials used to fabricate them and the possible interaction between these parts and the fluids/biological systems of interest. Typical microfluidic systems consist of four main components: (1) microfluidic pumps for driving the fluids along the system (based on various actuation mechanisms), (2) microfluidic valves for controlling and directing the flow as desired, (3) microfluidic channels and chambers, which are the passive and the primary fluidic interconnecting components of these systems, and (4) active microfluidic components integrated with closed-loop temperature controllers, optical detectors, electrodes for the application of test voltages and currents, and so forth [3].

### 1.3 Fabrication of microfluidics devices

Most microfluidic devices are fabricated by replica molding techniques [30, 31] because it allows for simple, low-cost prototyping of micro channels. Fig. 2 shows a typical fabrication procedure of a microfluidic chip. The polydimethylsiloxane (PDMS) microchannel is replicated from an SU-8 [32] photoresist negative pattern. Holes for tube connection are then mechanically punched through the channel. The channel is fixed onto a substrate, which often is a glass slide. There are several techniques for bonding the top micro channel and the bottom substrate. Typically, the PDMS part is O<sub>2</sub> plasma treated and pressed onto the glass substrate at 100°C to create permanent bonding. Simple mechanical clamps are also commonly used. Techniques for microchannel fabrication based on lithography include bulk micromachining of silicon. Anisotropic wet etching [33, 34] or DRIE [35, 36] creates grooves on silicon substrates. Other techniques include hot embossing [37] and injection molding [38], which are suitable for mass production [4].

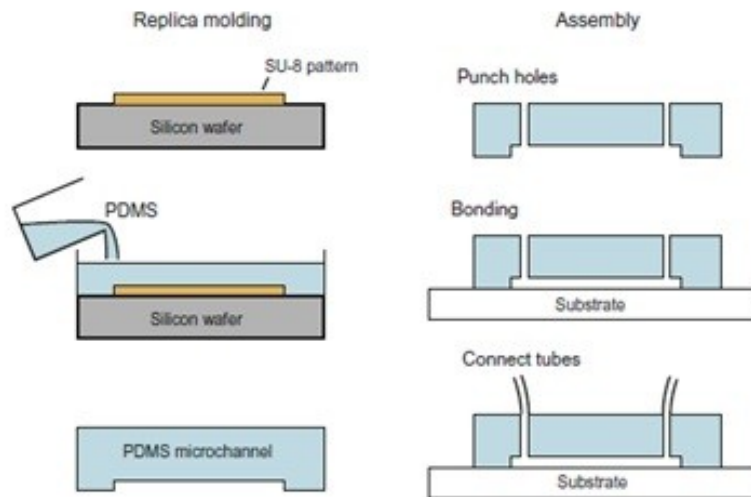


**Figure 2.** Fabrication of a PDMS microchannel [4].

### 1.4 Microfluidics

Microfluidics is the field of the microsystems technology that deals with the study and control of fluids in hydraulically/geometrically small systems, with lengths typically in the range of a few micrometers up to a few millimeters or centimeters [3, 4, 39]. It is an enabling technology to perform biological and chemical experiments at greatly reduced spatial scales, with minimal material consumption and high-throughput. It is based on the control of flows in microchannels with characteristic dimensions ranging from millimeters to micrometers, constituting the basis of technologies known as micro total analysis systems ( $\mu$ TAS) or labs-on-a-chip (LOC) [4].

Microfluidics is key to advancing molecular sensors based on bioassays including immunoassay, cell separation, DNA amplification, and analysis, among many other examples. Microfluidic systems process a large number of parallel experiments rapidly with a small amount of reagent and automate chemical, biological, and medical applications on a large scale with low cost. For example, reducing the reaction chamber size by a factor of 10 increases the reaction rate by a factor of 100 because the smaller characteristic length of the system decreases diffusion time. In addition to faster reaction times, the amounts of analyte and reagents required are also reduced proportionally to the reduction of the reaction chamber volume. Not only does this reduce the cost of the test by reducing the required amounts of chemicals, it also allows more types of tests to be conducted in parallel with the same size of sample [4].

### 1.5 Biochips

Materials used in microfluidic and biological applications must fulfill a stringent list of requirements. Biocompatibility is probably the most important one. The entire bill of materials need to be able to operate without releasing toxic chemicals, reacting with the fluids being transported and analyzed, or activate unwanted immunological response in the biological systems under analysis [40, 41]. Optical transparency is also a requirement for visualization of the flow using a microscope or video camera, enabling the identification and measurement of particles, cells, fluorescence, and the use of other colorimetric detection methods [3].

Biochips are based on the biological recognition and allow for the simultaneous analysis of a large number of compounds [42]. The discussed technology demands the application of very small amounts of starting material that minimizes the analysis cost [42]. Due to their advantages, the biochips have been applied for the determination of various diagnostic markers [43]

and genetic pre-disposition to many diseases [44]. Also, they have been successfully used in different practical fields such as molecular biology [45], medicine [46], biotechnology [47], etc [48].

The most important part of obtaining the final product is the production and subsequent functionalization of microfluidics by the specified production methods. Because all living things try to adapt to their environment in order to sustain their lives by perceiving the changes in the environment they live in [49]. Advances in basic sciences have enabled the investigation of the functions of other biological materials as well as enzymes [50]. As a result, a wide variety of microfluidic systems have been developed and are being developed.

In microfluidic device studies, enzyme fixation (immobilization) in the biological sensing region of the design is an important step. The most commonly used methods for enzyme immobilization in studies include; arresting in gel, intramolecular crosslinking, adsorption, covalent binding and encapsulation (Fig. 3) [49, 51].

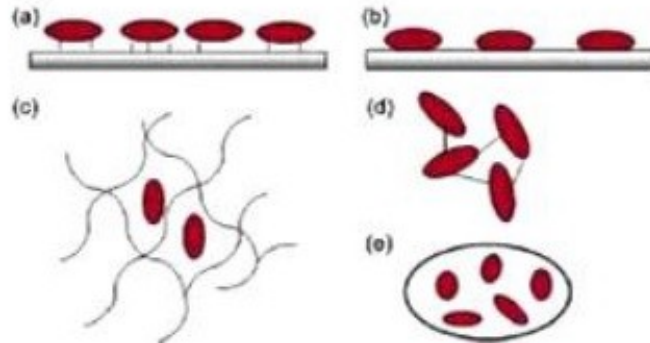


**Figure 3.** Enzyme Immobilization Methods, a) Covalent Binding, b) Adsorption, c) Arresting in Gel, d) Cross-Linking in Molecules, e) Encapsulation [49].

We prepared two types of biochips using polydimethylsiloxane (PDMS, Sylgard 184, Dow corning, Midland/USA) and perfluoropolyether (PFPE) urethane dimethacrylate (Fomblin MD40, Solvey Solexis, Milan/Italy). The design and dimensions of biochip have been described previously [52]. Briefly, the biochip consists of cell culture chamber manufactured with two layers. The microstructured bottom layer, with series of microchambers and microchannels, is used as a support for cell attachment. The second PDMS layer, with a reservoir (depth of 100  $\mu\text{m}$ ), is placed on top of the first layer and includes an inlet and outlet microfluidic network for homogenous culture medium distribution [53].

### 1.6 Wearable microfluidics chips

As a combination of wearable technology and microfluidics, wearable microfluidics directly contacts human skin, by which it enables the collection and analysis of body fluid as well as integration with wireless data transfer function. The wearable microfluidic chips can achieve the real-time continuous vital signs monitoring of glucose [54], lactate [55],  $\text{Na}^+/\text{K}^+$  [56],  $\text{Ca}_2^+$  [57] and pH of sweat [58], with the collection and analysis of sweat, interstitial fluid, saliva and tears. For the analysis of glucose and lactate, instead of directly collecting blood, with the help of wearable microfluidics technology, the minimally invasive and non-invasive sample collection methods could be used to ease patients' pain. Besides the advantages in sample collections, other advantages of wearable microfluidics are as follows: (1) the volume of the body fluid sample needed is much less compared with traditional methods; (2) the volume of the reagent needed for each test is also lowered to micro/nano liter scale, which significantly reduces the cost of each analysis; (3) the real-time and continuous in vivo monitoring of body fluid and wireless data transfer [59] could be achieved, which is almost impossible for traditional in vitro analysis method; (4) the wearable microfluidics can be easily integrated with other kinds of sensors since the fabrication technology of microfluidics is inherited from the microelectromechanical systems (MEMS). Sensors such as optical sensor, electrochemical sensor, piezoelectric sensor and biosensors can be integrated in the wearable microfluidics chips to meet different requirements of testing body fluid with much less technical barrier [29].

### 1.7 Exercise

Since physical exercise is a factor contributing to the quality of life of people, it is recommended as a very important prescription for both health and disease therapy [60]. The main purpose of exercise; to prevent organic and physical disorders caused by an inactive life and to maintain physical fitness for many years [61]. It is stated that there are physiological, motoric, psychological and sociological benefits in regular sports [61, 62, 63]. According to many studies, the increase in the physical activity of the individuals decreases the risk of death and prolongs the human life [60, 61]. In addition, the type of exercise, intensity, contests, traumas, stress cause both physiological and metabolic changes in the human body [60]. Therefore, the relationship between athletic performance, heavy exercise and physiological changes needs to be well known.

## 1.8 Methods for microfluidic cell separation

### I. Immunoassay-based methods

- i. Flow cytometry, fluorescence-activated cell sorting (FACS)
- ii. Magnetic separation, magnetic-activated cell sorting (MACS)
- iii. Affinity-mediated separation

### II. Utilization of electrical properties

- i. Electrophoresis

### III. Utilization of mechanical properties

- i. Acoustic separation
- ii. Size-based separation (hydrodynamics microfilters, centrifugation)

### IV. Stiffness-based separation

## 2. APPLICATION OF MICROFLUIDICS CHIPS AND BIOCHIPS

Most of the energy required for the tissue and cell activity is source from the glucose in blood. For the maintenance of organ and tissue functionality, the glucose level should be kept at a certain range. Lactic acid is the final product of glycolysis. In medical filed, it is an important indication for the exercise load control, diabetic monitoring and the detection of sugar souced disease [29]. Currently, the most popular dection methods of blood glucose are either using fully automatic biochemical analyser or fast blood glucose meter [64]. Compared with traditional method for the test of glucose, the wearable microfluidics technology provides a minimally invasive or non-invasive method. The minimally invasive method refers to collection of blood using microneedles array, of which the length of needles would not reach the subcutaneous neural layer, and the subject can hardly feel the pain. Non-invasive method refers to the indirect testing of glucose from the interstitial fluid [65, 66].

Gowers et al. developed a 3D-printed wearable microfluidic system, which could conduct the on-line testing of glucose and lactic acid simultaneously. A minimally invasive method was used with a Food and Drug Administration (FDA)-approved clinical microdialysis probe for the analysis of glucose and lactic acid. Fig. 4 A shows the integration method of the probes and microfluidic chips, Fig. 4 B and Fig. 4 C illustrate the changes of glucose and lactic acid level during a cycling protocol [67].

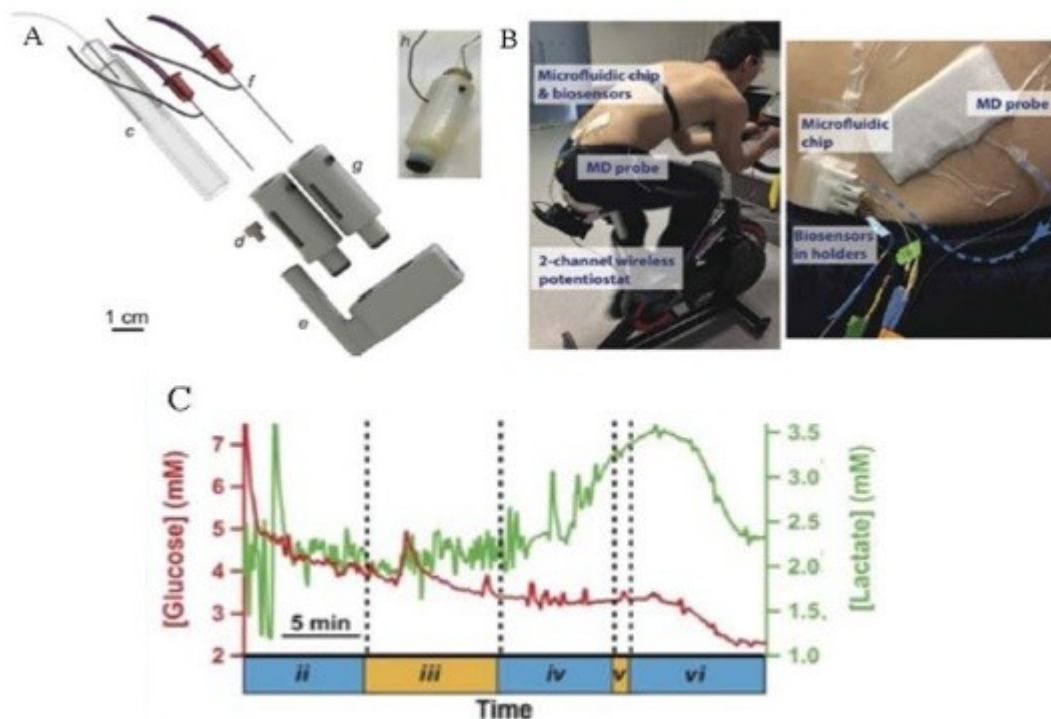


**Figure 4.** Wearable microfluidics system for glucose and lactic monitoring. (A) microfluidic device for continuous monitoring of dialysate; (B) measure tissue glucose and lactate levels in dialysate during the cycling protocol; (C) glucose and lactate levels during the exercise phase of the cycling protocol [67].

Perspiration is of great importance for maintaining the selfbalancing of inner environment of human body, and is also part of metabolism process. The sweat carries rich information, and real-time continues analysis of sweat is of great significance for the vital life sign monitoring. The pH value of sweat directly reflects the pH of human skin [29]. The change of pH in sweat also reflects the volume and speed during the perspiration processes, and the pH of sweat will increase when more sweat is produced [68]. On the basis of measuring pH value of sweat, we can indirectly speculate the dehydration of the subject, which is useful in the sports science and military field [29].

Traditional methods for testing pH in sweat require strenuous exercise to produce sweat, and then the sweat sample is collected for the chemical color reaction and the pH value is read out. This testing method requires the subject to produce significant amount of sweat, and is slow in detection and hard to realize continues real-time monitoring of pH value of sweat. On the other hand, using wearable microfluidics can realize real-time monitoring of pH of sweat and consume extra low sample and reagent volume [29].

Curto et al. proposed a simple and rapid wearable microfluidic devices for the testing of pH of sweat [58]. They used phosphonium based ionogel integrated with pH sensitive dyes for the direct testing of pH in sweat. Compared with other detection methods [69, 70], for example, photoelectric sensor to detect chromogenic reaction of pH in sweat, their method was low-cost with less energy consumption. As shown in Fig. 5 A, the structure of the proposed microfluidic devices was consisted of the absorbent pad for sweat, microchannels for sweat transfer and ionogel sensors for the chromogenic reaction of pH in sweat. Fig. 5 B shows the fabrication process of the microfluidic chips. The multiple layers of polymethyl methacrylate (PMMA), ionogel, and pressure-sensitive adhesive (PSA) were fabricated using  $CO_2$  laser and bonded using PSA. As shown in Fig. 5 C, the microfluidics chip was worn on human wrist. During the exercise, the color change of the ionogel could indicate the change of sweat pH in the range of 4.5 to 8.0 [58].

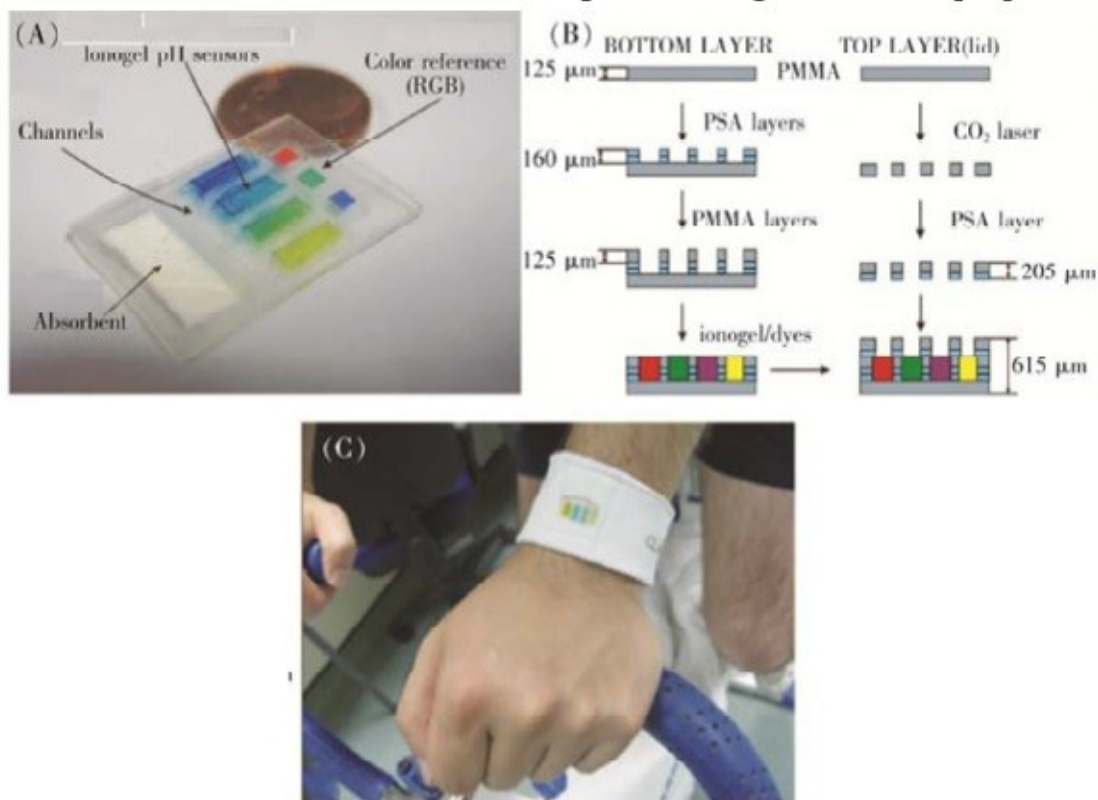


**Figure 5.** Wearable microfluidic system for sweat pH monitoring. (A) Image of the micro-fluidic platform; (B) micro-fluidic platform fabrication process; (C) image of the micro-fluidic system integrated into a wrist-band [58].

Coyle et al. fabricated a wearable microfluidic system that integrated the textile-based microfluidics for fluid transportation and a series of sensors for the analysis of sweat, including pH sensor [71]. Similar to Coyle's idea, Caldara et al. fabricated a wearable, flexible and non-toxic sweat sensor using the chromogenic reaction of organically modified silicate (ORMOSIL) [72]. As shown in Fig. 6, Tsioris et al. innovatively used the functionalized silk which had chromogenic reaction under different pH and integrated the silk in a PDMS-based microfluidic device for testing pH [73].

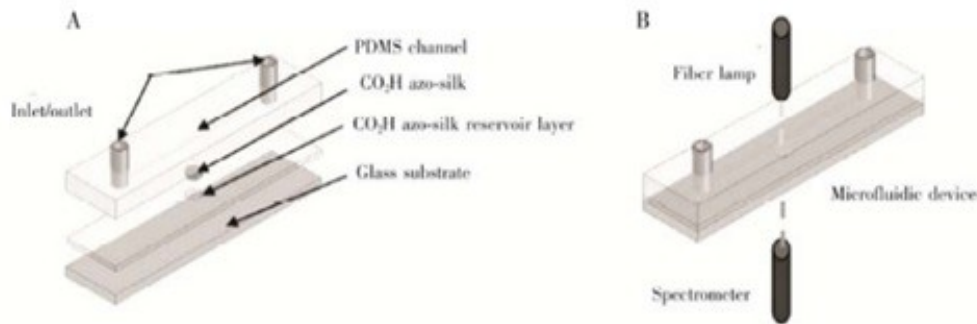


**Figure 6.** Structure of polydimethylsiloxane (PDMS)-based wearable microfluidic system for sweat pH monitoring. (A) Schematic of the microfluidic device composed of the PDMS channel, the  $CO_2H$  azo-silk, and an inlet/outlet; (B) optofluidic device setup [73].

The  $Na^+$  and  $K^+$  can directly reflect the hydration of human skin, the dehydration status and losses of electrolytes for the personal (athlete, coal miner, soldier) working in extreme environment (i.e. hot and humid) by monitoring the  $Na^+$  and  $K^+$  in sweat. In the severe environment with high temperature and humid, the sweating is the major way for the cooling of body, however, the sweating caused loss of electrolytes. If the body cannot adjust the environment well enough, the accumulated loss of  $Na^+$  (higher than 40 mM) will finally lead to muscle cramps or even heat stroke. Thus, monitoring the concentration of  $Na^+$  and  $K^+$  is of great importance for the health of people working in severe environment. It is worth to mention that during the body fluid testing, the concentrations of  $Na^+$  and  $K^+$  are also related to the pH value of the body fluid. Thus the simultaneous detection of ionic concentration and pH value is usually required [57].

As shown in Fig. 7, Matzeu et al. assembled dual ion-selective electrodes on the polyethylene terephthalate (PET) layer of a seven-layer microfluidic devices (Fig. 7 A), the polymethyl methacrylate (PMMA) and pressure sensitive adhesive (PSA) layers in this microfluidic chip were fabricated using  $CO_2$  laser ablation (Fig. 7 B), the PSA layers were used for the bonding between layers [56]. In this study, the researchers analyzed the relations of the output voltage and the concentration of  $Na^+$  using different electrode materials in the stationary cycling sessions (Fig. 7 C). A miniaturized wireless system was also developed in this study for the data transfer [56].

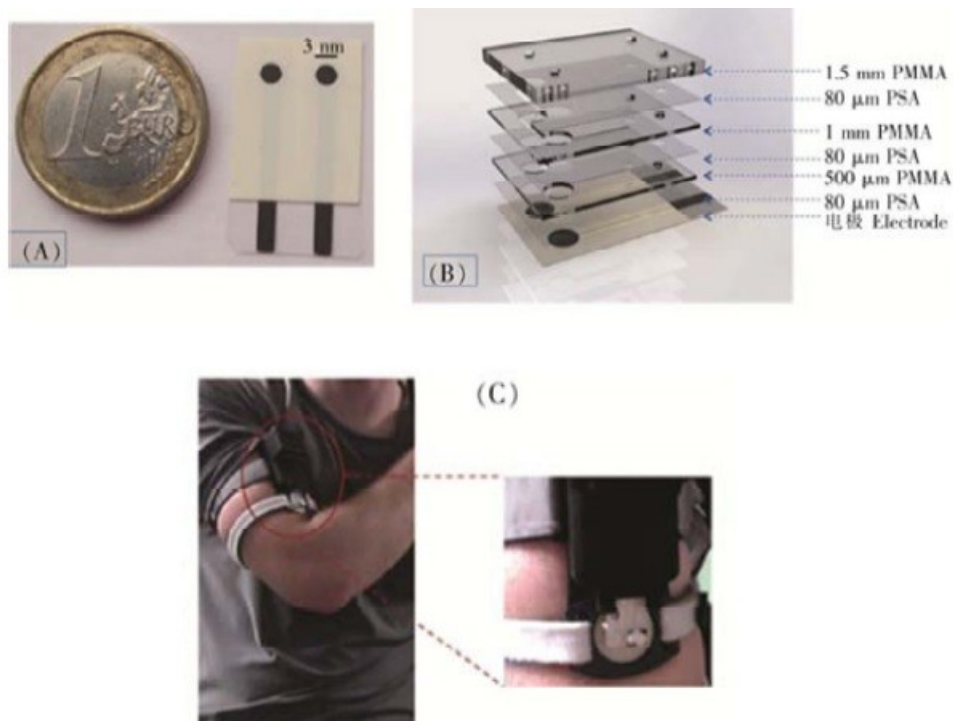


**Figure 7.** Polymer-based multi-layer wearable microfluidic system for sweat  $Na^+$  monitoring. (A) Dual screen-printed electrodes on a polyethylene terephthalate (PET) substrate; (B) different layers employed to build up the microfluidics collecting system; (C) microfluidic chip positioned on the upper arm of the subject [56].

Nyein et al. used ion-selective electrodes to detect  $Ca_2^+$  and pH value in sweat simultaneously [57].  $Ca_2^+$  detection electrode was made with a combination of organic membrane containing neutral carrier calcium (ETH 129) and an ion-selection transducer. The wearable microfluidic devices were attached to a flexible printed circuit board which handled the single process and wireless data transmission. The sensitivity for  $Ca_2^+$  was as high as 33.7 mV per decade [57].

Ingber et al. developed a microfluidic device which removes magnetized *Escherichia coli* bacteria from flowing solutions containing red blood cells [74]. The same group also demonstrated a blood cleansing device that removes *Candida albicans* fungi from flowing human whole blood with over 80% clearance at a flow rate of 20 mL/h [75]. Furdui et al. reported an integrated silicon microchip for separation of Jurkat cells from reconstituted horse blood samples as well as human blood (about 1:10,000 ratio of Jurkat cells to blood cells) [76]. Zborowski et al. demonstrated the separation of MCF7 cells (breast cancer cell line) from mixtures of human leukocytes [77].

## REFERENCES

- [1] Feynman, R. P. (1992). There's plenty of room at the bottom [data storage]. *Journal of microelectromechanical systems*, 1(1), 60-66.
- [2] Moore, G. E. (1998). Cramming more components onto integrated circuits. *Proceedings of the IEEE*, 86(1), 82-85.
- [3] Zahn, J. D. (2010). *Methods in Bioengineering Biomicrofabrication and Biomicrofluidics*, Artech House, ISBN-13: 978-1-59693-400-9.
- [4] Zhang, J. X., & Hoshino, K. (2018). *Molecular Sensors and Nanodevices: Principles, Designs and Applications in Biomedical Engineering*. Academic Press.
- [5] Wang, J., Pumera, M., Chatrathi, M. P., Escarpa, A., Konrad, R., Griebel, A., Dörner, W., & Löwe, H. (2002). Towards disposable lab-on-a chip: Poly (methylmethacrylate) microchip electrophoresis device with electrochemical detection. *Electrophoresis*, 23(4), 596-601.
- [6] Chin, C. D., Linder, V., & Sia, S. K. (2007). Lab-on-a-chip devices for global health: Past studies and future opportunities. *Lab on a Chip*, 7(1), 41-57.
- [7] Madou, M. J. (2011). *Manufacturing techniques for microfabrication and nanotechnology (Vol. 2)*. CRC press.
- [8] Rebeiz, G. M. (2004). *RF MEMS: theory, design, and technology*. John Wiley & Sons.
- [9] Neukermans, A., & Ramaswami, R. (2001). MEMS technology for optical networking applications. *IEEE Communications Magazine*, 39(1), 62-69.
- [10] Lin, L. Y., & Goldstein, E. L. (2002). Opportunities and challenges for MEMS in lightwave communications. *IEEE Journal of selected topics in quantum electronics*, 8(1), 163-172.
- [11] Wang, W., & Soper, S. A. (2006). *Bio-MEMS: technologies and applications*. CRC press.
- [12] Tabeling, P. (2005). *Introduction to microfluidics*. Oxford University Press on Demand.
- [13] Mastrangelo, C. H., Burns, M. A., & Burke, D. T. (1998). Microfabricated devices for genetic diagnostics. *Proceedings of the IEEE*, 86(8), 1769-1787.
- [14] Santini, Jr, J. T., Richards, A. C., Scheidt, R., Cima, M. J., & Langer, R. (2000). Microchips as controlled drug-delivery devices. *Angewandte Chemie International Edition*, 39(14), 2396-2407.
- [15] Thomas, D. J., Tehrani, Z., & Redfearn, B. (2016). 3-D printed composite microfluidic pump for wearable biomedical applications. *Additive Manufacturing*, 9, 30-38.
- [16] Su, W., Cook, B. S., & Tentzeris, M. M. (2016). Additively manufactured microfluidics-based "peel-and-replace" RF sensors for wearable applications. *IEEE Transactions on Microwave Theory and Techniques*, 64(6), 1928-1936.

- [17] Raya, R., Roa, J. O., Rocon, E., Ceres, R., & Pons, J. L. (2010). Wearable inertial mouse for children with physical and cognitive impairments. *Sensors and Actuators A: Physical*, 162(2), 248-259.
- [18] Lin, C. S., Hsu, H. C., Chiu, C. C., Lin, S. L., & Chao, C. S. (2006). A PDA based wearable system for real-time monitoring of human falls. *IETE journal of research*, 52(6), 403-416.
- [19] Georga, E. I., Protopappas, V. C., Bellos, C. V., & Fotiadis, D. I. (2014). Wearable systems and mobile applications for diabetes disease management. *Health and Technology*, 4(2), 101-112.
- [20] Hsu, Y. L., Chung, P. C., Wang, W. H., Pai, M. C., Wang, C. Y., Lin, C. W., Wu, H. L., & Wang, J. S. (2014). Gait and balance analysis for patients with Alzheimer's disease using an inertial-sensor-based wearable instrument. *IEEE journal of biomedical and health informatics*, 18(6), 1822-1830.
- [21] Mukhopadhyay, S. C. (2014). Wearable sensors for human activity monitoring: A review. *IEEE sensors journal*, 15(3), 1321-1330.
- [22] Attal, F., Mohammed, S., Dedabrishvili, M., Chamroukhi, F., Oukhellou, L., & Amirat, Y. (2015). Physical human activity recognition using wearable sensors. *Sensors*, 15(12), 31314-31338.
- [23] Taylor, G. S., & Barnett, J. S. (2013). Evaluation of wearable simulation interface for military training. *Human factors*, 55(3), 672-690.
- [24] Venkatraman, S., & Yuen, S. G. J. (2015). U.S. Patent No. 8,998,815. Washington, DC: U.S. Patent and Trademark Office.
- [25] Yang, J., Wei, D., Tang, L., Song, X., Luo, W., Chu, J., Gao, T., Shi, H., & Du, C. (2015). Wearable temperature sensor based on graphene nanowalls. *Rsc Advances*, 5(32), 25609-25615.
- [26] He, H., Li, Y., Guan, Y., & Tan, J. (2015). Wearable ego-motion tracking for blind navigation in indoor environments. *IEEE Transactions on Automation Science and Engineering*, 12(4), 1181-1190.
- [27] Villa, F., Magnani, A., Maggioni, M., Stahn, A., Rampichini, S., Merati, G., & Castiglioni, P. (2016). Wearable multi-frequency and multi-segment bioelectrical impedance spectroscopy for unobtrusively tracking body fluid shifts during physical activity in real-field applications: a preliminary study. *Sensors*, 16(5), 673.
- [28] Karuei, I., Schneider, O. S., Stern, B., Chuang, M., & MacLean, K. E. (2014). RRACE: Robust realtime algorithm for cadence estimation. *Pervasive and Mobile Computing*, 13, 52-66.
- [29] Yi-Qiang, F. A. N., Feng, G. A. O., Mei, W., Zhuang, J., Gang, T., & Zhang, Y. J. (2017). Recent development of wearable microfluidics applied in body fluid testing and drug delivery. *Chinese Journal of Analytical Chemistry*, 45(3), 455-463.
- [30] Whitesides, G. M. (2006). The origins and the future of microfluidics. *Nature*, 442(7101), 368.
- [31] McDonald, J. C., Duffy, D. C., Anderson, J. R., Chiu, D. T., Wu, H., Schueller, O. J., & Whitesides, G. M. (2000). Fabrication of microfluidic systems in poly (dimethylsiloxane). *ELECTROPHORESIS: An International Journal*, 21(1), 27-40.
- [32] Lorenz, H., Despont, M., Fahrni, N., LaBianca, N., Renaud, P., & Vettiger, P. (1997). SU-8: a low-cost negative resist for MEMS. *Journal of Micromechanics and Microengineering*, 7(3), 121.
- [33] Haneveld, J., Jansen, H., Berenschot, E., Tas, N., & Elwenspoek, M. (2003). Wet anisotropic etching for fluidic 1D nanochannels. *Journal of micromechanics and microengineering*, 13(4), S62. [34] Nilsson, A., Petersson, F., Jönsson, H., & Laurell, T. (2004). Acoustic control of suspended particles in micro fluidic chips. *Lab on a Chip*, 4(2), 131-135.
- [35] Jiang, L., Mikkelsen, J., Koo, J. M., Huber, D., Yao, S., Zhang, L., Zhou, P., Maveety, J. G., Prasher, R., Santiago,

- J. G., Goodson, K. E., & Kenny, T. W. (2002). Closed-loop electroosmotic microchannel cooling system for VLSI circuits. *IEEE Transactions on Components and Packaging Technologies*, 25(3), 347-355.
- [36] Di Carlo, D., Jeong, K. H., & Lee, L. P. (2003). Reagentless mechanical cell lysis by nanoscale barbs in microchannels for sample preparation. *Lab on a Chip*, 3(4), 287-291.
- [37] Becker, H., & Heim, U. (2000). Hot embossing as a method for the fabrication of polymer high aspect ratio structures. *Sensors and Actuators A: Physical*, 83(1-3), 130-135.
- [38] McCormick, R. M., Nelson, R. J., Alonso-Amigo, M. G., Benvegna, D. J., & Hooper, H. H. (1997). Microchannel electrophoretic separations of DNA in injection-molded plastic substrates. *Analytical Chemistry*, 69(14), 2626-2630.
- [39] Taylor, R. F., & Schultz, J. S. (Eds.). (1996). *Handbook of chemical and biological sensors*. CRC Press.
- [40] Williams, D. (2003). Revisiting the definition of biocompatibility. *Medical device technology*, 14(8), 10-13.
- [41] Freitas Jr, R. A. (2003). *Nanomedicine, Vol. IIA: Biocompatibility*. Karger Publishers.
- [42] Sutandy, F. R., Qian, J., Chen, C. S., & Zhu, H. (2013). Overview of protein microarrays. *Current protocols in protein science*, 72(1), 27-1.
- [43] Feyzkhanova, G. U., Filippova, M. A., Talibov, V. O., Dementieva, E. I., Maslennikov, V. V., Reznikov, Y. P., Offermann, N., Zasedatelev, A. S., Rubina, A. Y., & Fooke-Achterrath, M. (2014). Development of hydrogel biochip for in vitro allergy diagnostics. *Journal of immunological methods*, 406, 51-57.
- [44] Chang, Y. T., Yeh, Y. S., Ma, C. J., Huang, C. W., Tsai, H. L., Huang, M. Y., Cheng, T. L., & Wang, J. Y. (2017). Optimization of a multigene biochip for detection of relapsed and early relapsed colorectal cancer. *Journal of surgical research*, 220, 427-437.
- [45] Leclerc, E., Hamon, J., Legendre, A., & Bois, F. Y. (2014). Integration of pharmacokinetic and NRF2 system biology models to describe reactive oxygen species production and subsequent glutathione depletion in liver microfluidic biochips after flutamide exposure. *Toxicology in vitro*, 28(7), 1230-1241.
- [46] Kemmler, M., Sauer, U., Schleicher, E., Preininger, C., & Brandenburg, A. (2014). Biochip point-of-care device for sepsis diagnostics. *Sensors and Actuators B: Chemical*, 192, 205-215.
- [47] Chiang, Y. C., Wang, H. H., Ramireddy, L., Chen, H. Y., Shih, C. M., Lin, C. K., & Tsen, H. Y. (2018). Designing a biochip following multiplex polymerase chain reaction for the detection of *Salmonella* serovars Typhimurium, Enteritidis, Infantis, Hadar, and Virchow in poultry products. *Journal of food and drug analysis*, 26(1), 58-66.
- [48] Volokitina, M., Krutyakova, M., Sirotov, V., Larionov, M., Tennikova, T., & Korzhikova-Vlakh, E. (2019). Protein biochips based on macroporous polymer supports: Material properties and analytical potential. *Journal of pharmaceutical and biomedical analysis*, 165, 242-250.
- [49] Aydın, Y. (2012). İletken polimerlerin içerisinde enzim tutuklamasıyla yapılan biyosensörler (Yüksek Lisans Tezi, Karamanoğlu Mehmetbey Üniversitesi, Fen Bilimleri Enstitüsü).
- [50] Sassolas, A., Blum, L. J., & Leca-Bouvier, B. D. (2012). Immobilization strategies to develop enzymatic biosensors. *Biotechnology advances*, 30(3), 489-511.
- [51] Gulrajani, M. L., & Deepti, G. (2011). Emerging techniques for functional finishing of textiles.
- [52] Baudoin, R., Griscom, L., Prot, J. M., Legallais, C., & Leclerc, E. (2011). Behavior of HepG2/C3A cell cultures in a microfluidic bioreactor. *Biochemical Engineering Journal*, 53(2), 172-181.

- [53] Jellali, R., Paullier, P., Fleury, M. J., & Leclerc, E. (2016). Liver and kidney cells cultures in a new perfluoropolyether biochip. *Sensors and Actuators B: Chemical*, 229, 396-407.
- [54] Pu, Z., Zou, C., Wang, R., Lai, X., Yu, H., Xu, K., & Li, D. (2016). A continuous glucose monitoring device by graphene modified electrochemical sensor in microfluidic system. *Biomicrofluidics*, 10(1), 011910.
- [55] Kim, J., Valdés-Ramírez, G., Bandodkar, A. J., Jia, W., Martinez, A. G., Ramírez, J., Mercier, P., & Wang, J. (2014). Non-invasive mouthguard biosensor for continuous salivary monitoring of metabolites. *Analyst*, 139(7), 1632-1636.
- [56] Matzeu, G., O'Quigley, C., McNamara, E., Zuliani, C., Fay, C., Glennon, T., & Diamond, D. (2016). An integrated sensing and wireless communications platform for sensing sodium in sweat. *Analytical Methods*, 8(1), 64-71.
- [57] Nyein, H. Y. Y., Gao, W., Shahpar, Z., Emaminejad, S., Challa, S., Chen, K., Fahad, H. M., Tai, L. C., Ota, H., Davis, R. W., & Javey, A. (2016). A wearable electrochemical platform for noninvasive simultaneous monitoring of Ca<sup>2+</sup> and pH. *ACS nano*, 10(7), 7216-7224.
- [58] Curto, V. F., Fay, C., Coyle, S., Byrne, R., O'Toole, C., Barry, C., Hughes, S., Moyna, N., Diamond, D., & Benito-Lopez, F. (2012). Real-time sweat pH monitoring based on a wearable chemical barcode micro-fluidic platform incorporating ionic liquids. *Sensors and Actuators B: Chemical*, 171, 1327-1334.
- [59] Liu, G., Ho, C., Slappey, N., Zhou, Z., Snelgrove, S. E., Brown, M., Grabinski, A., Guo, X., Chen, Y., Miller, K., Kaya, T., & Edwards, J. (2016). A wearable conductivity sensor for wireless real-time sweat monitoring. *Sensors and Actuators B: Chemical*, 227, 35-42.
- [60] Laranjeiro, R., Harinath, G., Burke, D., Braeckman, B. P., & Driscoll, M. (2017). Single swim sessions in *C. elegans* induce key features of mammalian exercise. *BMC biology*, 15(1), 30.
- [61] Hartman, J. H., Smith, L. L., Gordon, K. L., Laranjeiro, R., Driscoll, M., Sherwood, D. R., & Meyer, J. N. (2018). Swimming exercise and transient food deprivation in *Caenorhabditis elegans* promote mitochondrial maintenance and protect against chemical-induced mitotoxicity. *Scientific reports*, 8(1), 8359.
- [62] Asthana, J., Yadav, A. K., Pant, A., Pandey, S., Gupta, M. M., & Pandey, R. (2015). Specioside ameliorates oxidative stress and promotes longevity in *Caenorhabditis elegans*. *Comparative Biochemistry and Physiology Part C: Toxicology & Pharmacology*, 169, 25-34.
- [63] Chuang, H. S., Kuo, W. J., Lee, C. L., Chu, I. H., & Chen, C. S. (2016). Exercise in an electrotactic flow chamber ameliorates age-related degeneration in *Caenorhabditis elegans*. *Scientific reports*, 6, 28064.
- [64] Bruen, D., Delaney, C., Florea, L., & Diamond, D. (2017). Glucose sensing for diabetes monitoring: recent developments. *Sensors*, 17(8), 1866.
- [65] Rebrin, K., Sheppard, N. F., & Steil, G. M. (2010). Interstitial Fluid Physiology as it Relates to Glucose Monitoring Technologies: Use of Subcutaneous Interstitial Fluid Glucose to Estimate Blood Glucose: Revisiting Delay and Sensor Offset. *Journal of Diabetes Science and Technology*, 4(5), 1087-1098.
- [66] Keenan, D. B., Mastrototaro, J. J., Weinzimer, S. A., & Steil, G. M. (2013). Interstitial fluid glucose time-lag correction for real-time continuous glucose monitoring. *Biomedical signal processing and control*, 8(1), 81-89.
- [67] Gowers, S. A., Curto, V. F., Seneci, C. A., Wang, C., Anastasova, S., Vadgama, P., Yang, G.Z., & Boutelle, M. G. (2015). 3D printed microfluidic device with integrated biosensors for online analysis of subcutaneous human microdialysate. *Analytical chemistry*, 87(15), 7763-7770.
- [68] Granger, D., Marsolais, M., Burry, J., & Laprade, R. (2003). Na<sup>+</sup>/H<sup>+</sup> exchangers in the human eccrine sweat duct. *American Journal of Physiology-Cell Physiology*, 285(5), C1047-C1058.

- [69] Schyrr, B., Pasche, S., Scolan, E., Ischer, R., Ferrario, D., Porchet, J. A., & Voirin, G. (2014). Development of a polymer optical fiber pH sensor for on-body monitoring application. *Sensors and Actuators B: Chemical*, 194, 238-248.
- [70] Yan, L., Chang, Y. N., Yin, W., Liu, X., Xiao, D., Xing, G., Zhao, L., Gu, Z., & Zhao, Y. (2014). Biocompatible and flexible graphene oxide/upconversion nanoparticle hybrid film for optical pH sensing. *Physical Chemistry Chemical Physics*, 16(4), 1576-1582.
- [71] Coyle, S., Lau, K. T., Moyna, N., O’Gorman, D., Diamond, D., Di Francesco, F., Costanzo, D., Salvo, P., Trivella, M. G., De Rossi, D. E., & Taccini, N. (2010). BIOTEX—Biosensing textiles for personalised healthcare management. *IEEE Transactions on Information Technology in Biomedicine*, 14(2), 364-370.
- [72] Caldara, M., Colleoni, C., Guido, E., Re, V., & Rosace, G. (2016). Optical monitoring of sweat pH by a textile fabric wearable sensor based on covalently bonded litmus-3-glycidoxypropyltrimethoxysilane coating. *Sensors and Actuators B: Chemical*, 222, 213-220.
- [73] Tsioris, K., Tilburey, G. E., Murphy, A. R., Domachuk, P., Kaplan, D. L., & Omenetto, F. G. (2010). Functionalized-Silk-Based Active Optofluidic Devices. *Advanced Functional Materials*, 20(7), 1083-1089.
- [74] Xia, N., Hunt, T. P., Mayers, B. T., Alsberg, E., Whitesides, G. M., Westervelt, R. M., & Ingber, D. E. (2006). Combined microfluidic-micromagnetic separation of living cells in continuous flow. *Biomedical microdevices*, 8(4), 299.
- [75] Yung, C. W., Fiering, J., Mueller, A. J., & Ingber, D. E. (2009). Micromagnetic–microfluidic blood cleansing device. *Lab on a Chip*, 9(9), 1171-1177.
- [76] Furdui, V. I., Kariuki, J. K., & Harrison, D. J. (2003). Microfabricated electrolysis pump system for isolating rare cells in blood. *Journal of Micromechanics and Microengineering*, 13(4), S164.
- [77] Fang, B., Zborowski, M., & Moore, L. R. (1999). Detection of rare MCF-7 breast carcinoma cells from mixtures of human peripheral leukocytes by magnetic deposition analysis. *Cytometry: The Journal of the International Society for Analytical Cytology*, 36(4), 294-302.

# Photochemical Reaction of Metal Carbonyls $[M(CO)_6 (M = Cr, Mo, W)]$ with 2-acetyl-5-chlorothiophenemethanesulfonylhydrazone

Sema SERT <sup>\*1</sup> , Ümmühan ÖZDEMİR ÖZMEN<sup>2</sup> 

## Abstract

The new complexes,  $[M(CO)_5(msh4)](Cr(1), Mo(2), W(3))$ , have been synthesized by the photochemical reaction of metal carbonyls with 2-acetyl-5-chlorothiophenemethanesulfonylhydrazone(msh4). The structure of these complexes has been investigated by using elemental analyses; FT-IR; EI-MS and <sup>1</sup>H NMR spectrometric methods. According to all spectroscopic data, msh4 is monodentate and coordinate via thiophene ring sulfur.

## Keywords

Metal carbonyls; Methanesulfonylhydrazone; Photochemical Reactions.

<sup>1</sup>Ege Üniversitesi, Fen Fakültesi, Kimya Bölümü, Bornova, İzmir, TÜRKİYE

<sup>2</sup>Gazi Üniversitesi, Fen-Edebiyat Fakültesi, Kimya Bölümü, Teknikokullar, Ankara, TÜRKİYE

\*Corresponding Author: semasertkimya@hotmail.com

Manuscript received date: September 24, 2018

Accept Date: November 28, 2018

Published Date: June 30, 2019.

## 1. INTRODUCTION

The importance of sulfonamide was reported to be the first antibacterial drug [1, 2]. Many sulfonylamide derivatives exhibit a cytostatic effect and find application in cancer chemotherapy [3, 6]. Methanesulfonamide residue has appeared as a suitable pharmacophoric equivalent to replace functional groups in drug design. Many compounds containing a hydrazine fragment, e.g. carboxylic acid hydrazides and their Schiff bases, have shown cytostatic activity [7]. Methanesulfonic acid (msh),  $CH_3SO_2NHNH_2$ , is the simplest organic representative of the compounds containing both sulfonamide and hydrazine. Structure and vibrational spectroscopy of msh were reported by Lenco et al. [8].

The literature is rich with transition metal-thiophene complexes containing thiophene ligands bound in many ways (i.e.  $\eta^1$ ,  $\eta^2$ ,  $\eta^3$ ,  $\eta^4$ ,  $\eta^5$ , and  $\eta^6$ ) to a variety of metal centers, but organometallic complexes of group VIB metals containing thiophene ligands are still relatively rare. Only two Mo complexes containing coordinated thiophene ligands have been reported. The first reported stable Mo-thiophene complex,  $[Mo(CO)_3(2,5-(Ph_2PCH_2CH_2)_2C_4H_2S)]$ , exists as a pair of chelating ligands that are bound to Mo through the phosphine groups and sulfur. The second complex,  $[Mo(\eta^6-2MeBT)_2]$ , is a sandwich complex consisting of a Mo coordinated to two 2-methylbenzothiophene (2-MeBT) ligands through the arene rings in an  $\eta^6$  fashion [9].

As ligands, methanesulfonylhydrazones, thiophene-2-carboxyaldehyde methane sulfonylhydrazone (msh 1), 2-acetyl thiophene methane sulfonyl hydrazone (msh 2), and 2-acetyl-5-methyl thiophene methane sulfonyl hydrazone (msh 3) and their metal carbonyl complexes have reported. In addition, structure and vibrational spectroscopy of msh, msh 1, msh 2, and msh 3 were reported [10].

In this work, first, the synthesis of 2-acetyl-5-chlorothiophenemethanesulfonylhydrazone (msh 4) were reported. Then, the new complexes  $[M(CO)_5(msh4)](M = Cr(1), Mo(2), W(3))$  as shown Figure 1 were prepared by the photochemical reactions of  $[M(CO)_6](M = Cr, Mo, W)$  with msh 4 and characterized elemental analysis, mass spectrometry, IR, and <sup>1</sup>H NMR spectroscopy. According to all the spectroscopic data, msh 4 is monodentate and coordinated via thiophene ring sulfur (C-S-C) in the complexes. Analytical data of the complexes are given in the experimental section.

## 2. EXPERIMENTAL SECTION

### 2.1 Materials and instrumentation

Elemental analysis was performed using LECO-CHNS-O-9320 model (TUBİTAK Laboratories, ANKARA). The infrared spectra of the compounds were recorded on samples in hexane at the Ege University with a Mattson 1000 FT-IR spectrometer.  $^1\text{H}$  NMR spectra were recorded in DMSO- $d_6$  on a 400 MHz High Performance Digital FT-NMR at TUBİTAK. Electron impact mass spectra were recorded on a Micromass VG Platform-II LC-MS at TUBİTAK. UV irradiations were performed with a medium-pressure 400 W mercury lamp through a quartz-walled, immersion-well reactor.

The solvents, pentane, benzene, hexane, dichloromethane, acetone, ethyl alcohol, diethylether, hydrazine hydrate, and silica gel were purchased from Merck and  $M(\text{CO})_6$  ( $M = \text{Cr}, \text{Mo}, \text{W}$ ) from Aldrich. These reagents were used as supplied. Methane sulfonyl chloride, hydrazine mono hydrate, and 2-acetyl-5-chlorothiophene were commercial products (purum). The solvents used were purified and distilled according to routine procedures [11].

### 2.2 Preparation of heteroaromatic methanesulfonylhydrazone

The preparation of heteroaromatic methanesulfonylhydrazone 4 is similar to that applied by Dodoff [12]. Thus, solution of 2.20 g (0.02 M) of msh is dissolved in 10 mL of ethanol. Then, the solution that 3.00 g (0.03 M) of the corresponding carbonyl compound (2-acetyl-5-chlorothiophene) dissolved in 10 mL of ethanol is added. The mixture is stirred for 30 min. The precipitating product is kept overnight in a deep freeze and then filtered. The precipitate is recrystallized from water and filtered, followed by rinsing with ether. Finally, it is dried on  $\text{P}_2\text{O}_5$  in a vacuum desiccator.

#### 2.2.1 Synthesis of 2-acetyl-5-chlorothiophenemethanesulfonylhydrazone (msh 4):

Yield(76%). Anal. Calcd. C, 33.28; N, 11.08; S, 25.38; H, 3.56. Found C, 35.42; N, 11.22; S, 25.46; H, 3.72. IR ( $\nu$ , KBr): 3198(s, NH), 3036(w,  $\text{CH}_{\text{ring}}$ ), 1600(m, CN), 1331(s,  $(\text{SO}_2)_{\text{asym}}$ ), 1170(s,  $(\text{SO}_2)_{\text{sym}}$ ), 896(m,  $\text{CSC}_{\text{ring}}$ ), 704(m,  $\text{CS}_{\text{sym}}$ ), 590(m,  $\text{CS}_{\text{asym}}$ ).  $^1\text{H}$  NMR ( $\delta$ , DMSO) = 2.20 ( $\text{CH}_3\text{C} = \text{N}$ , 3H, s); 3.01 ( $\text{CH}_3\text{SO}_2$ , 3H, s); 7.10 ( $\text{CH}_{\text{ring}}$ , 1H, s); 7.24 ( $\text{CH}_{\text{ring}}$ , 1H, s); 9.98 (NH, 1H, s).

### 2.3 Synthesis of metal carbonyl complexes

The complexes,  $[M(\text{CO})_5(\text{msh4})]$  ( $M = \text{Cr}(1), \text{Mo}(2), \text{W}(3)$ ) were prepared by photochemical reactions metal carbonyls  $M(\text{CO})_6$  ( $M = \text{Cr}, \text{Mo}, \text{W}$ ) with msh 4 and were obtained in 70-80% yields. The methods employed for the preparations of the complexes are very similar, so that the preparation of  $[\text{Cr}(\text{CO})_5(\text{msh4})](1)$  is given in detail as a representative example.

#### 2.3.1 $\text{Cr}(\text{CO})_5(\text{msh4})(1)$ :

$\text{Cr}(\text{CO})_6$  (0.44g, 2 mM) and msh4 (0.25g, 1 mM) were dissolved in tetrahydrofuran (80-100 mL). The solution was irradiated for 2 h using a 400 W medium-pressure mercury lamp through a quartz-walled immersion well reactor. During the irradiation, the color of the reaction mixture changed from colorless to light Brown. After irradiation, the reaction mixture was evaporated under vacuum, yielding a light brown solid. After dissolving in dichloromethane (10 mL), 50 mL of petroleum ether was added, resulting in precipitation of a light brown solid which was washed with petroleum ether and dried under vacuum. Traces of unreacted hexacarbonylchromium were sublimed out in vacuum on a cold finger at  $-20^\circ\text{C}$ . The composition of compounds is confirmed by elemental analysis. Yield: (76%). Found (%): C, 32.96; H, 2.40; N, 6.72; S, 14.88. Calcd. for  $\text{CrC}_{12}\text{H}_9\text{N}_2\text{O}_7\text{S}_2\text{Cl}$  (%): C, 32.41; H, 2.02; N, 6.30; S, 14.4. IR ( $\nu$ , KBr): 2070(w, CO), 1938(br, CO), 1880(sh, CO), 950(s,  $\text{CSC}_{\text{ring}}$ ), 868(m,  $\text{CSC}_{\text{ring}}$ ), 620(m,  $\text{CS}_{\text{sym}}$ ), 570(s,  $\text{CS}_{\text{asym}}$ )  $\text{cm}^{-1}$ .  $^1\text{H}$  NMR ( $\delta$ , DMSO- $d_6$ ): 2.18 ( $\text{CH}_3\text{C} = \text{N}$ , 3H, s); 3.01 ( $\text{CH}_3\text{SO}_2$ , 3H, s); 7.14 ( $\text{CH}_{\text{ring}}$ , 1H, s); 7.35 ( $\text{CH}_{\text{ring}}$ , 1H, s); 9.96 (NH, 1H, s) ppm. MS(LC, 70 eV):  $m/z$ (%) = 402(18)[ $\text{M}^+(\text{Me}^+\text{CO})$ ]; 374(20)[ $\text{M}^+(\text{Me}-2\text{CO})$ ]; 346(16)[ $\text{M}(\text{Me}-3\text{CO})$ ]; 318(10)[ $\text{M}^+(\text{Me}-4\text{CO})$ ]; 290(12)[ $\text{M}^+(\text{Me}-5\text{CO})$ ].

#### 2.3.2 $\text{Mo}(\text{CO})_5(\text{msh4})(2)$ :

A similar synthetic procedure as that used for 1 was used expect that  $\text{Cr}(\text{CO})_6$  was replaced by  $\text{Mo}(\text{CO})_6$ , giving pale-yellow crystals. Yield(58%). Found(%): C, 30.12; H, 2.02; N, 6.04; S, 13.66.  $\text{MoC}_{12}\text{H}_9\text{N}_2\text{O}_7\text{S}_2\text{Cl}$  (%): C, 29.50; H, 1.84; N, 5.73; S, 13.12. IR ( $\nu$ , KBr): 2073(w, CO), 1940(br, CO), 1888(sh, CO), 957(s,  $\text{CSC}_{\text{ring}}$ ), 866(m,  $\text{CSC}_{\text{ring}}$ ), 620(m,  $\text{CS}_{\text{sym}}$ ), 578(s,  $\text{CS}_{\text{asym}}$ )  $\text{cm}^{-1}$ .  $^1\text{H}$  NMR ( $\delta$ , DMSO- $d_6$ ): 2.18 ( $\text{CH}_3\text{C} = \text{N}$ , 3H, s); 3.01 ( $\text{CH}_3\text{SO}_2$ , 3H, s); 7.16 ( $\text{CH}_{\text{ring}}$ , 1H, s); 7.34 ( $\text{CH}_{\text{ring}}$ , 1H, s); 9.98 (NH, 1H, s) ppm. MS(LC, 70 eV):  $m/z$ (%) = 446(20)[ $\text{M}^+(\text{Me}^+\text{CO})$ ]; 418(18)[ $\text{M}^+(\text{Me}-2\text{CO})$ ]; 390(21)[ $\text{M}^+(\text{Me}-3\text{CO})$ ]; 362(14)[ $\text{M}^+(\text{Me}-4\text{CO})$ ]; 334(10)[ $\text{M}^+(\text{Me}-5\text{CO})$ ].

#### 2.3.3 $\text{W}(\text{CO})_5(\text{msh4})(3)$ :

A similar synthetic procedure as that used for 1 was used expect that  $\text{Cr}(\text{CO})_6$  was replaced by  $\text{W}(\text{CO})_6$ , giving pale-yellow crystals. Yield(56%). Found(%): C, 25.88; H, 1.82; N, 4.96; S, 11.64.  $\text{WC}_{12}\text{H}_9\text{N}_2\text{O}_7\text{S}_2\text{Cl}$  (%): C, 25.00; H, 1.56; N, 4.85; S, 11.12. IR ( $\nu$ , KBr): 2072(w, CO), 1930(br, CO), 1880(sh, CO), 958(s,  $\text{CSC}_{\text{ring}}$ ), 868(m,  $\text{CSC}_{\text{ring}}$ ), 612(m,  $\text{CS}_{\text{sym}}$ ), 580(s,  $\text{CS}_{\text{asym}}$ )  $\text{cm}^{-1}$ .  $^1\text{H}$  NMR ( $\delta$ , DMSO- $d_6$ ): 2.18 ( $\text{CH}_3\text{C} = \text{N}$ , 3H, s); 3.01 ( $\text{CH}_3\text{SO}_2$ , 3H, s); 7.11 ( $\text{CH}_{\text{ring}}$ , 1H, s); 7.30 ( $\text{CH}_{\text{ring}}$ , 1H, s); 9.98 (NH, 1H, s) ppm.

s); 9.98 (NH, 1H, s) ppm. MS(LC, 70 eV):  $m/z(\%) = 533(15)[M^+-(Me^+CO)]$ ;  $505(22)[M^+-(Me-2CO)]$ ;  $477(20)[M^+-(Me-3CO)]$ ;  $449(10)[M^+-(Me-4CO)]$ ;  $421(10)[M^+-(Me-5CO)]$ .

### 3. RESULTS AND DISCUSSION

#### 3.1 Synthesis

The analytical results and some physical properties of the new heteroaromatic methanesulfonylhydrazone **msh 4** is summarized. It is colorless crystalline solid, stable at room temperature, and soluble in methanol, ethanol, THF,  $CH_2Cl_2$ , DMSO, and poorly soluble in benzene and water.

#### 3.2 Spectroscopic characterization

The assignment of the FTIR bands were made taking into consideration literature data for compounds containing appropriate structural fragments: sulfonamides [13, 17], sulfonyl hydrazines, and sulfonylhydrazones [12, 18, 20], methanesulfonyl derivatives [21, 24], and Schiff bases of salicylaldehyde, and related compounds [25, 29]. Infrared revealed that absorption due to C=O of the free ligand is  $1610-1590\text{ cm}^{-1}$  [12]. The N-H absorption appeared at  $3230-3180\text{ cm}^{-1}$ . The observed band at  $520-320\text{ cm}^{-1}$  correspond to C-Cl stretching vibrations [30]. The medium C-S-C asymmetric stretch is  $850-800\text{ cm}^{-1}$  [31].

$^1\text{H}$  NMR data of DMSO- $d_6$  solutions of the **msh 4** (2-acetyl-5-chlorothiophenemethanesulfonylhydrazone) is collected in the experimental section. The comparison of spectra of ketone derivatives facilitates distinguishing the signals of the methyl protons from  $CH_3-C$ ,  $CH_3C=N$ , and  $CH_3SO_2$  fragments, the assignment of the latter being in accord with the data reported [12]. The signal of the  $CH_3C=N$  protons show no splitting, and the positions of signals of the ring protons are typical.

The carbonyl complexes,  $[M(CO)_5(\text{msh4})]$  ( $M = Cr, Mo, W$ ) (**msh4** = 2-acetyl-5-chlorothiophenemethanesulfonylhydrazone) were prepared by a photochemical reaction as shown in Figure 1. The photogeneration of  $M(CO)_5$  from  $M(CO)_6$  ( $M = Cr, Mo, W$ ) has been extensively studied. These 16-electron  $M(CO)_5$  fragments react quickly with any available donor to form  $M(CO)_5L$  species. The spectroscopic studies show that **msh 4** monodentate coordinating via the thiophene ring sulfur (C-S-C) in the complexes. Analytical data of the complexes are given in the experimental section.

Important infrared spectral data of the complexes are presented in the synthesis section. Spectral shifts observed for a number of peaks in the vibrational spectra of **msh 4** ligand are significant. The medium intensity band at  $890\text{ cm}^{-1}$  observed in free ligand ascribed to  $\nu(CSC)_{ring}$  stretch is divided in two bands, to higher values with  $50\text{ cm}^{-1}$  and to lower values with  $50\text{ cm}^{-1}$  for all compounds, suggesting involvement of sulfur in the bonding with metal [32]. The bands assigned to symmetric  $\nu(C-S)$  and asymmetric  $\nu(C-S)$  shift to lower frequency after complexation in all complexes. No shifts were observed at  $\nu_{asym}(SO_2)$ ,  $\nu_{sym}(SO_2)$ ,  $\nu(NH)$ , and  $\nu(C=N)$  with complex formation showing that  $SO_2$ , NH, and C=N were not coordinated in the complexes.

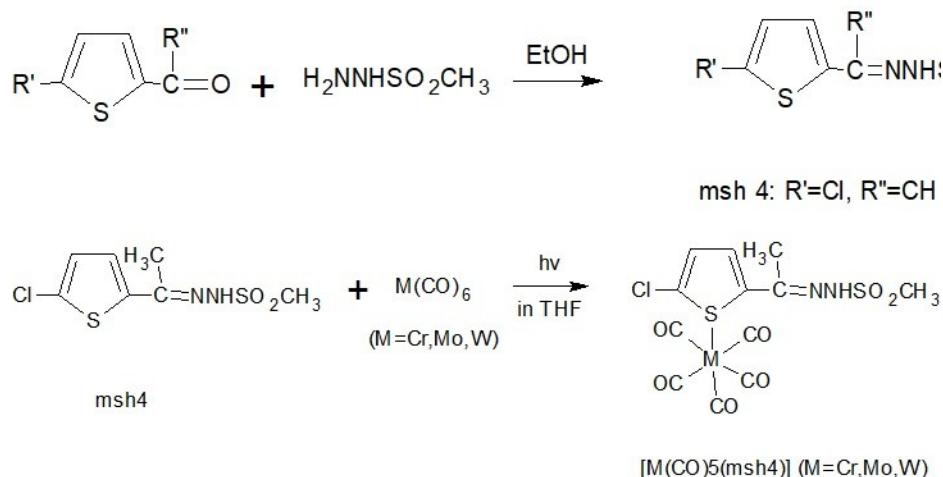


**Figure 1.** Synthesis of **msh 4** and the photochemical reaction of  $M(CO)_6$  ( $M = Cr, Mo, W$ ) with **msh 4**.

$^1\text{H}$  spectra in DMSO- $d_6$  solutions of compounds are reported in the experimental section. In the  $^1\text{H}$  NMR spectra, an upfield shift of about 0.11 ppm for the ring protons relative to the free ligand was observed. The small shift is related to a decrease in  $\pi$ -electron density in the ring protons with complex formation [33].

The mass spectra show fragmentation via successive loss of CO groups and organic ligands.

## Acknowledgement

We thank BP(Turkey) for the provision of photochemical apparatus and the Research Foundation of Ege and Gazi University. We thank TÜBİTAK for all allocation of time for NMR, mass spectra and elemental analyses.

## REFERENCES

- [1] G.Domagk, Deut. Med. Wochenschr. 61(1935) 250.
- [2] G.I.Mandell, W.A.Petri, J.G.Hardman, L.E.Limbird, P.B.Molinoff, R.W.Ruddon, A.G.Gilman, Goodman's the Pharmacological Basis of Therapeutics, 9th ed., McGraw-Hill, New York, 1996.
- [3] N.R.Lomax, LV.L.Narayanan, Chemical Structures of Interest to the Division of Cancer Treatment, Vol. VI, Developmental Therapeutics Program, National Cancer Institute, Bethesda, MD, p.32(1988).
- [4] P.B.Jensen, B.S.Soerensen, J.F.E.Demant, M.Sehested, P.S.Jensen, L.H.Vindeloe, H.H.Hansen, Cancer Res., 50, 3311(1990).
- [5] G.J.Finlay, B.C.Baguley, K.Snow, W.Judd, J.Natl.Cancer Inst., 82, 662(1990).
- [6] S.Topiol, M.Sabio, P.W.Erhardt, J.Chem.Soc., Perkin Trans., 2, 437(1998).
- [7] H.Rutner, N.Lewin, E.C.Woodbury, T.J.McBride, K.V.Rao. Cancer Chemother.Rep., Part 1, 58, 803 (1974).
- [8] A.Lenco, C.Mealli, P.Paoli, N.Dodoff, Z.Kantarci, N.Karacan, New J. Chem., 23, 1253(1999).
- [9] M.A. Reynolds, A.A. Guzei, B.C. Logsdon, L.M. Thomas, R.A. Jacobson, R.J. Angelici. Organometallics, 18, 4075 (1999).
- [10] G.Orhan, O.S.Şentürk, Ü.Ö.Özmen, S.Sert, E.Subaşı, J.of Coord. Chem., 64, 19 (2014).
- [11] D.D.Perrin, W.F.F.Armarego, D.R.Perrin, Purification of Laboratory Chemicals, Pergamon Press, Oxford (1980).
- [12] N.I.Dodoff, Ü.Özdemir, N.Karacan, M.Georgieva, S.M.Konstantinov, M.E.Stefanova, Z.Naturforsch, 54b, 1553(1999).
- [13] K. Hanai, T. Okuda, T. Uno, K. Machida. Spectrochim. Acta, 31, 1217 (1975).
- [14] A.R. Katritzky, R.A. Jones. J. Chem. Soc., 4497 (1960)
- [15] N. Bacon, A.J. Boulton, R.T.C. Brownlee, A.R. Katritzky, R.D. Topsom. J. Chem. Soc., 5230 (1965).
- [16] Y. Tanaka, Y. Tanaka. Chem. Pharm. Bull., 13, 858 (1965).
- [17] K. Hanai, A. Noguchi, T. Okuda. Spectrochim. Acta, 34, 771 (1978).
- [18] Ü. Özdemir, O.S. Sentürk, S. Sert, N. Karacan, F. Uğur. Transit. Met. Chem., 28, 443 (2003).
- [19] Ü.Ö. Özdemir, N. Akkaya, N. Özbek. Inorg. Chim. Acta, 400, 13 (2013).
- [20] R.J.W. Cremllyn, D.N. Waters. J. Chem Soc., suppl. 2, 6243 (1964).
- [21] R.D. McLachlan, V.B. Carter. Spectrochim. Acta, 26, 1121 (1970).
- [22] T. Uno, K. Machida, K. Hanai. Spectrochim. Acta, 27, 107 (1971).
- [23] G. Geiseler, G. Hanschmann. J. Mol. Struct., 8, 293 (1971).
- [24] G. Chassaing, J. Corset, J. Limouzi. Spectrochim Acta, 37, 721 (1981).

- [25] P. Teyssie, J.J. Charette. *Spectrochim. Acta*, 19, 1407 (1963).
- [26] J.A. Faniran, K.S. Patel, J.C. Bailar Jr. *J. Inorg. Nucl. Chem.*, 36, 1547 (1974).
- [27] L.I. Kozhevina, E.B. Prokopenko, V.I. Rybachenko, E.V. Titov. *Zh. Prikl. Spektrosk.*, 59, 440 (1993).
- [28] V.I. Tsapkov, N.M. Samus'. *Zh. Obshch. Khim.*, 67, 1422 (1997).
- [29] P. Mills, S. Korlann, M.E. Bussell, M.A. Reynolds, M.V. Ovchinnikov, R.J. Angelici, C. Stinner, T. Weber, R. Prins. *J. Phys. Chem. A*, 105, 4418 (2001).
- [30] C.Kumar, C.Parlak, H.Fun, M.Tursun, G.Keşan, S.Chandrajou, C.K.Quah, *Spectrochim. Acta Part A: Molecular and Biomolecular Spectroscopy* 127,67 (2014).
- [31] P. Mills, S. Korlann, M.E. Bussell, M.A. Reynolds, M.V. Ovchinnikov, R.J. Angelici, C. Stinner, T. Weber, R. Prins. *J. Phys. Chem.*, 105, 4418 (2001).
- [32] C. Spinu, A. Kriza. *Acta Chim. Slov.*, 47, 179 (2000).
- [33] F. Sarıkahya, O.S. Şentürk. *Syn. React. Inorg. Met.*, 31, 1843 (2001).

# A Bioactive (2R, 3R)-dihydroflavonol-3-O- $\alpha$ -L-rhamnoside from *Brachystelma togoense* Schltr

Abiche Ekalu<sup>\*1</sup> , Rachael Gbekele-Oluwa Ayo<sup>2</sup> , James D. Habila<sup>2</sup>  and Ibrahim Hamisu<sup>2</sup> 

## Abstract

The Nigerian medicinal plant, *Brachystelma togoense* has being used to treat various ailments such as typhoid fever, cold and cough, gonorrhoea, skin infections, dysentery and pneumonia. In order to determine the ethnomedicinal potential of *Brachystelma togoense*. A dihydroflavonol-3-O- $\alpha$ -L-rhamnoside was isolated from the MeOH extract of the plant. The compound was identified using 1D and 2D NMR spectroscopic methods, mass spectrometry and by comparison with literature data. The compound exhibited antimicrobial activity against *Staphylococcus aureus*, *Streptococcus pneumoniae*, *Escherichia coli*, *Salmonella typhi*, and *Candida albicans* < 3 mg/ml. The compound had minimum inhibitory concentration ranging from 0.18 to 0.75 mg/ml and minimum bactericidal concentration ranging from 0.75 to 1.50 mg/ml. The compound is reported for the first time from *Brachystelma togoense*.

## Keywords

flavonoid; dihydroflavonol-3-O- $\alpha$ -L-rhamnoside; *Brachystelma togoense* schltr

<sup>1</sup>Nigerian Army School of Education, Ilorin, Kwara, Nigeria

<sup>2</sup>Ahmadu Bello University Zaria, Kaduna, Nigeria

\*Corresponding Author: ekalumiracle@gmail.com

Manuscript received date: May 25, 2019

Accept Date: June 25, 2019

Published Date: June 30, 2019.

## 1. INTRODUCTION

*Brachystelma* was first described by Robert Brown in 1822. The genus *Brachystelma* R. Br. (Apocynaceae: Asclepiadoideae) is represented by about 100-120 species (Bruyns, 2009). The genus *Brachystelma* is chiefly distributed in South Africa, South-East Asia and Australasia (Ollerton et al., 2009). A total of 18 species are known in India (Britto and Bruyns, 2016) and out of them, 3 species in Maharashtra. It is an erect perennial herb, growing up to 30 cm, recorded from Ghana to Nigeria, in lowlands to montane situations. The tuber is said to be edible raw (Kew Royal Botanical Gardens, 2019). Many of the tuberous *Brachystelma* are known to be used medicinally for the treatment of headache, stomach ache and colds in children.

The World Health Organization (WHO) has reported that traditional medicinal plants are those natural plant materials which are used without processing for the treatment of various ailments in our locality. Traditional herbal medicine has being in use for the past years because it is natural and have fewer side effects (Jamshidi-kia et al., 2018). In view of the uses of these plants for the treatment of various ailments that we decided to isolate the bioactive flavonoid in *B.togense*. Flavonoids are referred to as the primary class of polyphenolic compounds (Xie et al., 2015). Most flavonoids have been reported to exhibit various microbial activities which includes but not limited to anti-oxidation, anticancer, anti-inflammatory activities (Xiao and Kai, 2012). Over the years, flavonoids have become interesting subject of medical research all over the world. This is because, they have been reported to possess vast antimicrobial activities (Cushnie and Lamb, 2005). Flavonoids have been reported also to possess many biochemical properties. They are known for their antioxidant activity, hepatoprotective activity, antibacterial activity, anti-inflammatory activity, anticancer activity and antiviral activity (Kumar and Pandey, 2013). A similar flavonoid, 2-3-dihydromyricetin-3-O- $\alpha$ -L-rhamnoside isolated from *Pradosia huberi* (Ducke) Ducke (Sapotaceae) was reported for rat isolated mesenteric arteries though it was ineffective in the eliciting vasorelaxation (Medeiros et al., 2010). But flavonoid antimicrobial activities have been well documented. Therefore, the biological investigation of the plant which led to the

isolation and characterization of a bioactive flavonoid has justified the ethnomedicinal use of *B. togoense* in Nigeria.

## 2. MATERIALS and METHODS

### 2.1 Instrumentation

The NMR spectra were recorded in CD<sub>3</sub>OD on a 400 MHz Bruker AVANCE III NMR instrument at room temperature. HREIMS was recorded on an Agilent Technologies 6550 iFunnel Q-TOF LC/MS with the sample dissolved in CH<sub>2</sub>Cl<sub>2</sub>. The optical rotation was determined in CH<sub>2</sub>Cl<sub>2</sub> on a JASCO P-1020 polarimeter and the infrared spectra was recorded using a Perkin-Elmer (2000 FTIR) spectrometer on NaCl plates. The ECD spectra was measured on a Chirascan CD spectrometer using a 1 mm cell with acetonitrile as solvent at the Department of Chemistry, FEPS, University of Surrey, United Kingdom.

### 2.2 Plant material

The aerial parts of *Brachystelma togoense* was collected in the month of April 2018 from Benue State, Nigeria. The plant was identified by the plant taxonomist Mallam Sanusi Namadi and a voucher specimen (25856) is retained in Biological Science Department, Ahmadu Bello University, Zaria-Nigeria (Ekalu et al., 2019).

### 2.3 Extraction and isolation

The air dried *Brachystelma togoense* (1.0 kg) was extracted on a shaker at room temperature successively with 100 % CH<sub>3</sub>OH for 72 hours. The extracts was concentrated using a rotary evaporator at 40 °C to a yield brown gum (9.0 g, 0.9 % MeOH extract). The extract was separated by flash chromatography (Biotage SP1) over silica gel using three solvent mixtures; first with a CH<sub>2</sub>Cl<sub>2</sub>/EtOAc step gradient starting with 100 % CH<sub>2</sub>Cl<sub>2</sub> and gradually increasing the polarity to 100 % CH<sub>2</sub>Cl<sub>2</sub> then EtOAc was added gradually until 100 % EtOAc was reached to yield 8 fractions ((Fr.1-Fr.8). Fr.5 was separated successively over Sephadex LH-20 (CH<sub>3</sub>OHEtOAc 2:8) to give 1 (50 mg, 0.6 %).

### 2.4 Antimicrobial screening

The antimicrobial activities of the isolates were determined using some microorganisms. The microorganisms were obtained from the Department of Medical Microbiology, Ahmadu Bello University Teaching Hospital, Zaria, Nigeria. The antimicrobial activity of the isolates were evaluated using the broth dilution assay as described previously for the bacteria and Mueller Hinton broth assay for the fungus (Niaz et al., 2018). The microorganisms tested were: *Staphylococcus aureus*, *Streptococcus pneumoniae*, *Escherichia coli*, *Salmonella typhi*, and *Candida albicans*. Different solutions of 6.0 mg of the compound were made using DMSO (10 ml) and the experiment was also set up using DMSO as the control (Bello et al., 2011a).

### 2.5 Determination of zone of inhibition

The standardized inocula of the isolate were uniformly placed on freshly prepared Mueller Hinton agar plates using a sterile swab stick. Exactly 5 appropriately labelled wells were punched into each agar plate using a sterile cork borer (6 mm in diameter). Aliquot of 0.3 ml of the appropriate isolate concentration was placed in each well and then allowed to diffuse into the agar. An extra plate was streaked with the isolate and ciprofloxacin (10  $\mu$ /disc) was placed on it. The plates were incubated at 37 °C for 24 h. While for the fungus, Sabouraud dextrose broth was used and the incubation period was 30 °C and 48 h. The antimicrobial activities were expressed as diameter (mm) of inhibition zones produced by the isolate (Bello et al., 2011a).

### 2.6 Minimum inhibition concentration (MIC)

The minimum inhibition concentrations of the isolate was carried out using the broth dilution method as outlined by the Clinical and Laboratory Standards Institute (CLSI. Performing Standards for Antimicrobial Susceptibility Testing, Clinical and Laboratory Standards Institute, n.d.). Mueller Hinton broth was prepared; 10 ml was dispensed into tubes and was sterilized at 121 °C for 15 minutes and allowed to cool. The McFarland turbidity standard scale 0.5 was prepared to give turbidity solution. Normal saline was prepared, 10 ml was dispensed into sterile test tube and the test microbes was inoculated and incubated at 37 °C for 24 hours. Dilution of the test microbes was done in the normal saline until the turbidity matched that of the Mc-Farland turbidity scale by visual comparison at this point the test microbe has a concentration of about 1.5x10<sup>8</sup> cfu/mL. Two-fold serial dilution of the extracts in the sterilized broth was made to obtain the concentrations of 3.00 mg/ml, 1.50 mg/ml, 0.75 mg/ml, 0.37 mg/ml, 0.18 mg/ml and 0.09 mg/ml. The initial concentration was obtained by dissolving 6 mg of the isolate in 10 ml of the sterile broth. Having obtained the different concentrations of the extracts in the sterile broth, 0.3 ml of the standard inoculum of the test microbe in the normal saline was then inoculated into the different concentrations. Incubation was made at 37 °C for 24 h, after which each test tube of the broth was observed for turbidity (growth). The lowest concentration of the isolate in which the broth shows no turbidity was recorded as the Minimum Inhibition Concentration (MIC) (Bello et al., 2011a).

## 2.7 Determination of minimum bactericidal concentration/minimum fungicidal concentration (MBC/MFC)

This was carried out to determine whether the microorganisms could be completely killed or their growth could only be inhibited. The minimum bactericidal concentration of the isolates was determined as outlined by the CLSI on the nutrient agar plates. Minimum bactericidal concentrations were determined by assaying the test tube contents of the MIC determinations. A loopful of the content of each tube was inoculated by streaking on a solidified nutrient agar plate and then incubated at 37 °C for 24 h for bacterial and 30 °C for 48 h for fungus. Then it was observed for microbial growth. The lowest concentration of the subculture with no growth was the minimum bactericidal concentration/ minimum fungicidal concentration (Bello et al., 2011a).

## 3. RESULTS and DISCUSSION

### 3.1 Data for compound 1

Dihydroflavonol-3-O- $\alpha$ -L-rhamnoside (1): Yellow solid,  $[\alpha]_D^{20} = -83.6$  (c = 1.00, MeOH); HRESIMS: m/z 474.1071 [ $C_{21}H_{24}O_7 + Na$ ] (Calculated for  $C_{21}H_{24}O_7Na$  473.1060 for  $C_{21}H_{22}O_11Na$ ); IR (neat): 3382, 2919, 1638  $cm^{-1}$ ;  $^1H$  NMR ( $CD_3OD$ , 400 MHz) and  $^{13}C$  NMR ( $CD_3OD$ , 100 MHz) data are given in Table 1.

Compound 1 was isolated as a yellow solid from the MeOH extract of the aerial parts of *Brachystelma togoense* and was identified as the known dihydroflavonol-3-O- $\alpha$ -L-rhamnoside, which has been isolated from the methanol extract of Xinjiang wine grapes (*Vitis vinifera*) (De Britto et al., 1995; Xueyan et al., 2018).

The HRESIMS (spectrum 1.1) showed a molecular ion peak at m/z  $[M+H+Na]^+ = 474.1071$  (calcd 473.1060 for  $C_{21}H_{22}O_{11}Na$ ) indicating a molecular formula of  $C_{21}H_{22}O_{11}$  for the compound. The IR spectrum (spectrum 1.2) showed absorbance bands for hydroxyl (3382  $cm^{-1}$ ), conjugated ketone (1638  $cm^{-1}$ ),  $sp^3$  CH (2919 and 2851  $cm^{-1}$ ) and olefinic carbon (1463  $cm^{-1}$ ) groups.

Ring A showed meta-coupled H-6 ( $\delta_H$  5.93 d, J = 1.2 Hz) and H-8 ( $\delta_H$  5.91 d, J = 1.2 Hz) proton resonances and ring B showed an ABX system with coupled H-2' ( $\delta_H$  6.97 d, J = 1.9 Hz), H-5' ( $\delta_H$  6.83 d, J = 8.2 Hz) and H-6' ( $\delta_H$  6.84 dd, J = 2.1, 8.1 Hz) resonances. As no methoxy groups were present, hydroxyl groups were placed at C-5, C-7, C-3' and C-4'. Hydroxyl group proton resonances were not seen in the  $^1H$  NMR spectrum (spectrum 1.3) as the solvent used was deuterated methanol and the hydroxyl groups of the molecule undergo proton exchange.

A keto group ( $\delta_C$  196.1) was present in the  $^{13}C$  NMR spectrum (spectrum 1.4) that could be assigned to C-4 of the flavonoid skeleton. A pair of doublets ( $\delta_H$  5.09 d, J = 10.8 Hz,  $\delta_H$  4.59 d, J = 10.7 Hz) could be assigned to H-2 and H-3 of ring B. These large coupling constants showed that H-2 and H-3 were trans to each other.

The NMR spectra showed the presence of one sugar group. The presence of a three proton doublet ( $\delta_H$  1.19 d, J = 6.3 Hz) indicated that this was  $\alpha$ -L-rhamnose (Xueyan et al., 2018). This was supported by correlations seen in the NOESY spectrum (spectrum 1.9) between the 1'' ( $\delta_H$  4.06 d, J = 1.6 Hz), 3'' ( $\delta_H$  3.67 dd, J = 3.4, 9.5 Hz), 4'' ( $\delta_H$  3.31 dd, J = 6.6, 9.5 Hz) and 5'' ( $\delta_H$  4.26 dd, J = 6.5, 9.6 Hz) proton resonances. The rhamnose was attached at C-3  $\beta$ . This was shown by a correlation seen between the H-3 and C-1'' ( $\delta_C$  102.3) resonances.

The  $^1H$  and  $^{13}C$  NMR resonances were assigned using HSQC and HMBC spectra and are given in Table 1, the structure of compound 1 is shown in Figure 1.

The specific rotation was found to be  $[\alpha]_D^{20} = -83.6$  (c = 1.00 g/ml, MeOH) and  $[\alpha]_D^{20} = -13.5$  was reported (Xueyan et al., 2018) which confirmed the stereochemistry of compound 1. The configurations at the chiral centres were confirmed using the NOESY spectrum.

The ECD spectrum (spectrum 1.10) agreed with the stereochemistry reported in literature (De Britto et al., 1995).

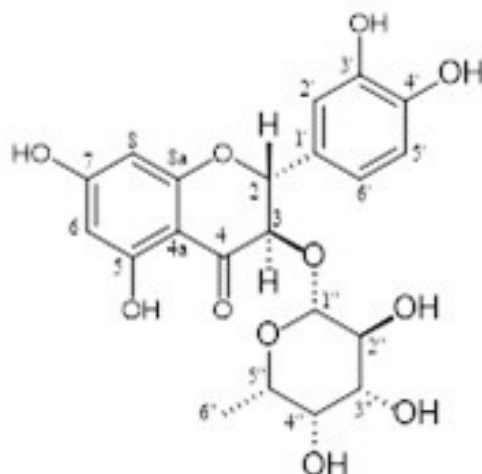


**Figure 1.** Molecular structure of (2R, 3R)-dihydroflavonol-3-O- $\alpha$ -L-rhamnoside isolated from *bracystelma togoense*.

**Table 1.** NMR Data for (2R, 3R)-dihydroflavonol-3-O- $\alpha$ -L-rhamnoside ( $CD_3OD$ , 400 MHz J in Hz)

C	$^{13}C$ NMR (100MHz) in $CD_3OD$	$^{13}C$ NMR (100MHz) in DMSO-6 (Xueyan et al., 2018)	$^1H$ NMR (400MHz) $CD_3OD$ (J in Hz)	HMBC (H $\rightarrow$ C)	COSY	NOESY
1	-	-	-	-	-	-
2	84.1 CH	82.4	5.09 d, J= 10.8	1', 2', 3, 4, 6'	3 $\alpha$	3
3	78.7 CH	76.5	4.59 d, J= 10.7	1', 1'', 2, 4	2 $\beta$	2
4	196.1 C	195.1	-	-	-	-
5	164.3 C	162.8	-	-	-	-
6	97.5 CH	96.2	5.93 d, J= 2.1	5, 7, 8	-	-
7	165.7 C	167.0	-	-	-	-
8	96.4 CH	95.1	5.91 d J= 2.1	6,7,9	-	-
4a	162.5 C	162.8	-	-	-	-
8a	102.6 C	101.5	-	-	-	-
1'	129.3 C	128.1	-	-	-	-
2'	115.6 CH	114.5	6.97 d, J= 1.9	1', 2, 3', 6'	-	-
3'	146.7 C	145.9	-	-	-	-
4'	147.5 C	145.1	-	-	-	-
5'	116.5 CH	115.2	6.83 d J= 8.2	1', 4', 6'	6'	-
6'	120.6 CH	119.5	6.84 dd, J = 2.1, 8.1	1', 2, 4', 5'	5'	-
1''	102.3 CH	100.5	4.06 d, J= 1.6	-	-	3 $\alpha$ , 3'', 4'', 5''
2''	71.9 CH	70.4	3.54 dd, J= 1.7, 3.3	-	-	3 $\alpha$ , 3'', 5''
3''	72.3 CH	71.3	3.67 dd, J = 3.4, 9.5	4'', 5''	4'', 5''	3 $\alpha$ , 4'', 5''
4''	73.9 CH	72.6	3.31 dd, J = 6.6, 9.5	3'', 5'', 6''	3'', 5'', 6''	2
5''	70.7 CH	68.9	4.26 dd, J = 6.5, 9.6	3'', 4'', 6''	3'', 4'', 6''	3 $\alpha$ , 3'', 4''
6''	17.9 CH3	17.1	1.19 d, J= 6.3	4'', 5''	4'', 5''	3 $\alpha$ , 3'', 4'', 5''

**Table 2.** Diameter of Zone of Inhibition (mm) of the compound

Micro organisms	Concentration (mg/ml)					Ciprofloxacin 10x10-6	Terbinafine 30x 10-6
	3.0	1.5	0.75	0.375			
<i>S. aureus</i>	16	14	13	12		25	
<i>E. coli</i>	18	16	14	13		35	
<i>S. pneumoniae</i>	16	14	12	11		20	
<i>S. typhi</i>	23	20	16	13		24	
<i>C. albicans</i>	20	18	16	14			

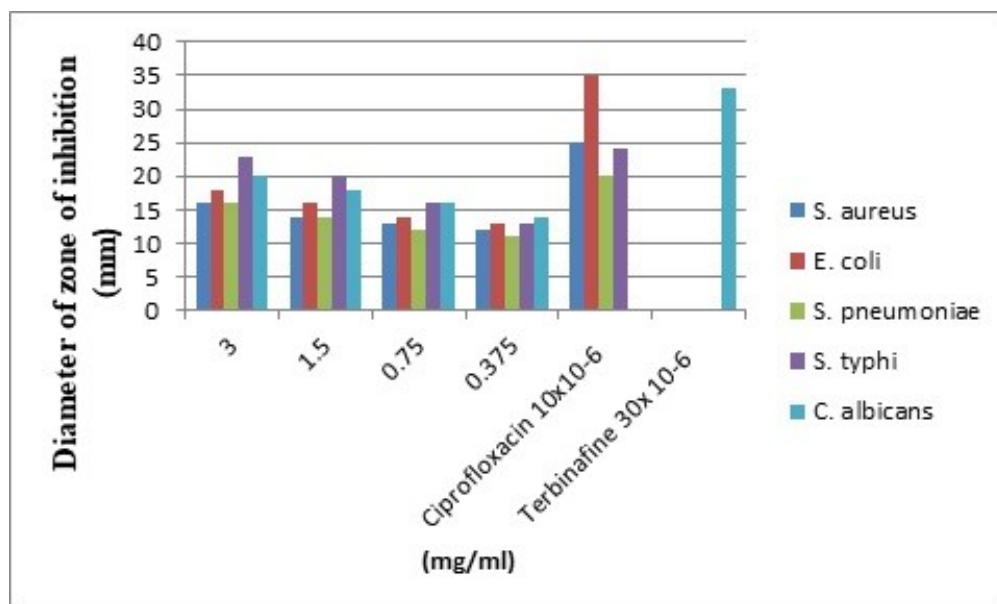


**Figure 2.** Representation of diameter of zone of inhibition.

**Table 3.** Summary of MIC, MBC and MFC of the compound (mg/ml)

Micro organisms	MIC	MBC	MFC
<i>S. aureus</i>	0.75	1.50	
<i>E. coli</i>	0.37	0.75	
<i>S. pneumoniae</i>	0.75	1.50	
<i>S. typhi</i>	0.37	0.75	
<i>C. albicans</i>	0.18		0.75

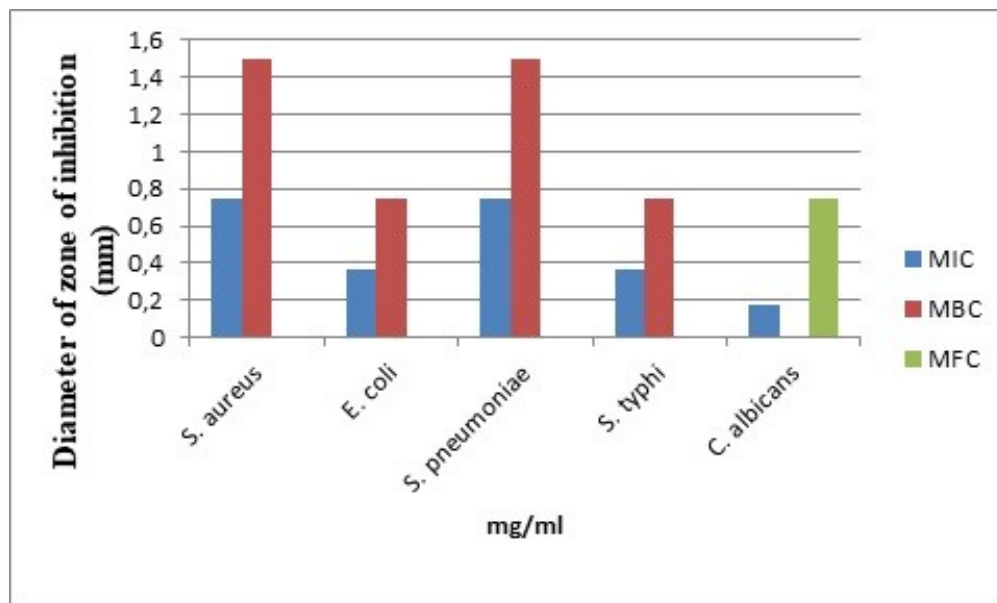


**Figure 3.** Representation of MIC, MBC and MFC of the compound (mg/ml).

Flavonoids are phenolics widely distributed in plants with reported antimicrobial activity (Cushnie and Lamb, 2005). The results showed that the compound had a remarkable activity against all the five microorganisms tested. Four bacterial strains, *Staphylococcus aureus*, *Streptococcus pneumoniae*, *Escherichia coli*, *Salmonella typhi*, were used. Ciprofloxacin was used as the positive control against the four bacteria with MIC values of 0.75, 0.37, 0.75, 0.37 mg/ml (Table 3 and figure 3) respectively.

*Candida albicans* was used as the fungus. Terbinafine was used as the positive control against the fungus with MIC values of 0.18 mg/ml (Table 3 and figure 3). The compound had zones of inhibition ranging from 11 to 23 mm (Table 2 and figure 2). Flavonoids have been reported to exhibit anti-inflammatory, anti-microbial, anti-cancer and anti-allergic activities (Bello et al., 2011b). The antimicrobial activity of flavonoid has been reported (Taleb-Contini et al., 2003) for different flavonoids on microorganisms. There, we can confirm that the isolated compound, a flavonoid has vast medicinal potential which justifies the ethnomedicinal uses of the plant.

#### **4. CONCLUSION**

A flavonoid was isolated and identified as a (2R, 3R)-dihydroflavonol-3-O- $\alpha$ -L-rhamnoside from *B.togoense*. To the best of our knowledge, the compound is reported for the first time in this source. The flavonoid showed significant activities against *E. coli*, *S. typhi* and *C. albicans*. The results from this research have supported the ethnomedicinal uses of this plant in the treatment of, typhoid fever skin infections, abdominal disorders, dysentery, pneumonia, gonorrhoea, and as a cough and cold remedy. This justifies the ethnomedicinal uses of the plant in Nigeria.

#### **Conflict of interest**

The authors declare no conflict of interest

#### **Acknowledgement**

This work was supported by Tertiary Education Trust Fund (TETFUND). The author wishes to thank the Natural product Research Group of the Department of Chemistry, University of Surrey, United Kingdom for the laboratory and NMR analyses.

#### **REFERENCES**

- Bello, I.A., Ndukwe, G.I., Audu, O.T., Habila, J.D., 2011a. A bioactive flavonoid from *Pavetta crassipes* K. Schum. *Organic and Medicinal Chemistry Letters* 1, 14. <https://doi.org/10.1186/2191-2858-1-14>
- Bello, I.A., Ndukwe, G.I., Audu, O.T., Habila, J.D., 2011b. A bioactive flavonoid from *Pavetta crassipes* K. Schum. *Organic and Medicinal Chemistry Letters* 1:14, 10–15. <https://doi.org/10.1186/2191-2858-1-14>
- Britto, S.J., Bruyns, P. V, 2016. Three new species of *Brachystelma* from Tamil Nadu, India. *Haseltonia* 48–54.
- Bruyns, P. V, 2009. Three New Species of *Brachystelma* (Apocynaceae, Asclepiadoideae, Ceropogonieae) from South Tropical and Southern Africa. *SPIE*.
- CLSI. *Performing Standards for Antimicrobial Susceptibility Testing*, Clinical and Laboratory Standards Institute, 2017:32, n.d. PL, 27 th. ed.
- Cushnie, T.P.T., Lamb, A.J., 2005. Antimicrobial activity of flavonoids. *International Journal of Antimicrobial Agents* 26, 343–356. <https://doi.org/10.1016/j.ijantimicag.2005.09.002>
- De Britto, J., Soosai Manickam, V., Gopalakrishnan, S., Ushioda, T., Tanaka, N., 1995. Chemical and chemotaxonomical studies of ferns. Determination of aglycone chirality in dihydroflavonol 3-O- $\alpha$ -L-rhamnosides by <sup>1</sup>H-NMR spectroscopy. <https://doi.org/10.1248/cpb.43.338>
- Ekalu, A., Ayo, R.G., Habila, J.D., Hamisu, I., 2019. Phaeophytin and Triterpenoids from *Brachystelma togoense* Schltr, a Nigerian Medicinal Herb. *Asian Journal of Chemical Sciences* 6, 1–5. <https://doi.org/10.9734/AJOCS/2019/v6i118990>
- Jamshidi-kia, F., Lorigooini, Z., Amini-khoei, H., 2018. Medicinal plants: Past history and future perspective. *Journal of Hermed Pharmacology* 7, 1-7. <https://doi.org/10.15171/jhb.2018.01>
- Kew Royal Botanical Gardens, 2019. Electronic Plant Information Centre (ePIC) [WWW Document]. URL <http://epic.kew.org/index.htm> (accessed 2.7.19).
- Kumar, S., Pandey, A.K., 2013. Chemistry and Biological Activities of Flavonoids: An Overview. *The Scientific World Journal*

2013, 1–3. [https://doi.org/10.1016/S1572-5995\(05\)80065-1](https://doi.org/10.1016/S1572-5995(05)80065-1)

Medeiros, A.A.N., Medeiros, F.A., Queiroz, T.M., Tavares, J.F., Silva, M.S., Medeiros, I.A., 2010. Artigo rhamnoside from *Pradosia huberi* (Ducke) Ducke on rat isolated mesenteric arteries. *Animals* 20, 542–548.

Niaz, S.I., Zhang, P., Shen, H., Li, J., Chen, B., Chen, S., Liu, L., He, J., 2018. Two new isochroman derivatives penisochromanes A and B from ascidian-derived fungus *Penicillium* sp. 4829. *Natural Product Research* 6419, 1–7. <https://doi.org/10.1080/14786419.2018.1470173>

Ollerton, J., Masinde, S., Meve, U., Picker, M., Whittington, A., 2009. Fly pollination in *Ceropegia* (Apocynaceae: Asclepiadoideae): biogeographic and phylogenetic perspectives. *Annals of Botany* 103, 1501–1514. <https://doi.org/10.1093/aob/mcp072>

Taleb-Contini, S.H., Salvador, M.J., Watanabe, E., Ito, I.Y., Oliveira, D.C.R. de, 2003. Antimicrobial activity of flavonoids and steroids isolated from two *Chromolaena* species. *Revista Brasileira de Ciências Farmacêuticas* 39, 403–408. <https://doi.org/10.1590/S1516-93322003000400007>

Xiao, J., Kai, G., 2012. A review of dietary polyphenol-plasma protein interactions: Characterization, influence on the bioactivity, and structure-affinity relationship. *Critical Reviews in Food Science and Nutrition* 52, 85–101. <https://doi.org/10.1080/10408398.2010.499999>

Xie, Y., Yang, W., Tang, F., Chen, X., Ren, L., 2015. Antibacterial activities of flavonoids: structure-activity relationship and mechanism. *Current medicinal chemistry* 22, 132–49. <https://doi.org/10.2174/0929867321666140916113443>

Xueyan, R., Jia, Y., Xuefeng, Y., Lidan, T., Qingjun, K., 2018. Isolation and purification of five phenolic compounds from the Xinjiang wine grape (*Vitis Vinifera*) and determination of their antioxidant mechanism at cellular level. *European Food Research and Technology* 244, 1569–1579. <https://doi.org/10.1007/s00217-018-3070-z>